

HIF-1 α induces glycolytic reprogramming in tissue-resident alveolar macrophages to promote cell survival during acute lung injury

31-01-2022-RA-eLife-77457R1

(Clean version)

¹Parker S. Woods, ¹Lucas M. Kimmig, ¹Kaitlyn A. Sun, ¹Angelo Y. Meliton,
¹Obada R. Shamaa, ¹Yufeng Tian, ¹Rengül Cetin-Atalay, ²Willard W. Sharp,
¹Robert B. Hamanaka, and ¹Gökhan M. Mutlu

Department of Medicine, ¹Section of Pulmonary and Critical Care Medicine, and ²Section of
Emergency Medicine, The University of Chicago, Chicago, IL 60637

Corresponding Author:

Gökhan M. Mutlu, MD
The University of Chicago
Section of Pulmonary and Critical Care Medicine
5841 S. Maryland Avenue
MC6026
Chicago, IL 60637
Phone: 773-702-1002
Fax: 773-702-6500
Email: gmutlu@medicine.bsd.uchicago.edu

33

34 **ABSTRACT**

35 Cellular metabolism is a critical regulator of macrophage effector function. Tissue-resident
36 alveolar macrophages (TR-AMs) inhabit a unique niche marked by high oxygen and low
37 glucose. We have recently shown that in contrast to bone marrow-derived macrophages
38 (BMDMs), TR-AMs do not utilize glycolysis and instead predominantly rely on mitochondrial
39 function for their effector response. It is not known how changes in local oxygen concentration
40 that occur during conditions such as acute respiratory distress syndrome (ARDS) might affect
41 TR-AM metabolism and function; however, ARDS is associated with progressive loss of TR-
42 AMs, which correlates with the severity of disease and mortality. Here, we demonstrate that
43 hypoxia robustly stabilizes HIF-1 α in TR-AMs to promote a glycolytic phenotype. Hypoxia
44 altered TR-AM metabolite signatures, cytokine production, and decreased their sensitivity to the
45 inhibition of mitochondrial function. By contrast, hypoxia had minimal effects on BMDM
46 metabolism. The effects of hypoxia on TR-AMs were mimicked by FG-4592, a HIF-1 α stabilizer.
47 Treatment with FG-4592 decreased TR-AM death and attenuated acute lung injury in mice.
48 These findings reveal the importance of microenvironment in determining macrophage
49 metabolic phenotype, and highlight the therapeutic potential in targeting cellular metabolism to
50 improve outcomes in diseases characterized by acute inflammation.

INTRODUCTION

Glycolytic metabolism has been ascribed a central role in macrophage inflammatory processes (Tannahill, Curtis et al. 2013, Freemerman, Johnson et al. 2014, Palsson-McDermott, Curtis et al. 2015, Xie, Yu et al. 2016, Ip, Hoshi et al. 2017). Much of our current understanding of this phenomena has been elucidated in bone marrow-derived macrophages (BMDMs) and macrophage cell lines (i.e., THP-1 and RAW 264.7), which model macrophages of monocytic lineage. Considerably less is known about how other factors like local microenvironment and developmental origin may influence macrophage metabolic function. Tissue-resident alveolar macrophages (TR-AMs) reside within the lumen of the lung alveolus where they are critical in maintaining lung homeostasis within the healthy airway and are the first responders to airborne pathogens and pollutants (Hussell and Bell 2014). The alveolus maintains the highest oxygen concentration of any tissue compartment within the human body (Carreau, El Hafny-Rahbi et al. 2011). Moreover, under steady-state conditions, glucose concentrations within the airway lumen are less than one-tenth of blood glucose concentrations (Baker, Clark et al. 2007). These environmental conditions alone suggest a requirement for oxidative metabolism for cells that reside within the alveoli. Several studies have demonstrated that the unique characteristics of the alveolar microenvironment heavily influence macrophage function and immunometabolism (Lavin, Winter et al. 2014, Svedberg, Brown et al. 2019, McQuattie-Pimentel, Ren et al. 2021). Our group has recently demonstrated that TR-AMs rely predominantly on oxidative phosphorylation under steady-state conditions and that glycolysis is dispensable for proinflammatory effector function in these cells (Woods, Kimmig et al. 2020). Together, these findings highlight the lung microenvironment's central role in dictating TR-AM responses.

Conditions associated with severe airway inflammation (i.e., acute respiratory distress syndrome (ARDS)) increase alveolar epithelial/endothelial barrier permeability (Ware and Matthay 2000). This results in flooding of alveoli with fluid and recruitment of non-resident

immune cells leading to severe local hypoxia as well as an increase in alveolar glucose levels (Fröhlich, Boylan et al. 2013, Campbell, Bruyninckx et al. 2014, Baker and Baines 2018). These abrupt changes in the alveolar microenvironment under a diseased state such as ARDS likely necessitate metabolic adaptation by TR-AMs in order to ensure optimal cellular fitness. Acute lung injury/ARDS is associated with a decline in the number of TR-AMs and the degree of TR-AM loss correlates with clinical outcomes (i.e., mortality) (Fan and Fan 2018). Moreover, experimental depletion of TR-AMs results in an increase in the severity of acute lung injury and mortality (Beck-Schimmer, Schwendener et al. 2005, Kim, Lee et al. 2008, Jaworska, Coulombe et al. 2014, Machado-Aranda, V Suresh et al. 2014, Nelson, Zhou et al. 2014, Schneider, Nobs et al. 2014, Cardani, Boulton et al. 2017). Whether or not changes in the alveolar microenvironment play a role in TR-AM cell death during acute lung injury/ARDS has yet to be explored.

Hypoxia-inducible factor 1-alpha (HIF-1 α) is the most extensively characterized transcription factor responsible for cellular adaptation to low oxygen levels (Semenza 2012). In brief, under normoxia, oxygen-dependent proline hydroxylases prevent HIF-1 α activation by marking it for proteasomal degradation. Conversely, under hypoxia, decreased hydroxylase activity promotes HIF-1 α protein stabilization and translocation to the nucleus allowing for transcriptional responses to low oxygen levels, such as enhanced expression of genes related to glycolysis and angiogenesis. HIF-1 α has been well characterized in macrophages of monocytic origin, and identified to play a key role in macrophage infiltration and proinflammatory responses (Cramer, Yamanishi et al. 2003, Peyssonnaud, Datta et al. 2005, Tannahill, Curtis et al. 2013, Matak, Heinis et al. 2015, Palsson-McDermott, Curtis et al. 2015). However, little is known about the role that HIF-1 α plays in TR-AM effector function and metabolism. In a study focusing on TR-AM development, the expression of HIF-1 α and its target genes was found to be turned off following birth and this process was required for TR-AM maturation and normal effector function

(Izquierdo, Brandi et al. 2018). It is unknown; however, whether HIF-1 α plays a role in TR-AM effector function after maturation or how local hypoxia and changes in the expression of HIF-1 α might regulate the adaptation of mature TR-AMs to hypoxia or affect their effector function during acute lung injury.

To answer these questions, we used a variety of metabolic and immunological approaches. We observed that HIF-1 α was undetectable in primary TR-AMs cultured under normoxia, but was robustly stabilized under hypoxia in a dose-dependent fashion. Upon hypoxic HIF-1 α stabilization, TR-AMs acquired a glycolytic phenotype, which was not observed under normoxic conditions. In contrast, BMDMs exhibited no alterations in HIF-1 α stabilization or glycolytic output in response to hypoxia. Analysis of LPS-induced TR-AM metabolite signatures revealed significant increases in glycolytic intermediates under hypoxia. Hypoxia also altered the TR-AM cytokine profile in response to LPS and was able rescue the ETC inhibitor-induced impairment in cytokine production in TR-AMs.

Using influenza infection in mice to model acute lung injury, we found that TR-AM cell number decreased over the course of acute lung injury. Surviving TR-AMs exhibited a glycolytic gene signature supporting hypoxic adaptation. To determine how the ability to adapt to hypoxia affects TR-AM survival and function, we treated influenza-infected mice intratracheally with FG-4592, a HIF-1 α stabilizer, which mimics hypoxic adaptation. Compared to control mice, FG-4592 prevented the loss of TR-AMs, reduced lung injury, and increased survival. Collectively, our data suggest that HIF-1 α plays a critical role in TR-AM metabolic adaptation to altered environmental conditions during acute lung injury. Promoting hypoxic adaptation and glycolytic metabolism in TR-AMs enables them to adapt to and survive the changes in the microenvironment during lung injury and consequently reduces lung inflammation and may offer

128 a viable therapeutic strategy in treating ARDS arising from influenza or other severe viral
129 infections, including COVID19.

RESULTS

Tissue-resident alveolar macrophages exhibit HIF-1 α stabilization and develop a glycolytic phenotype in response to hypoxia

We have recently shown that TR-AMs maintain a very low glycolytic rate which is not augmented by activation of inflammatory responses (Woods, Kimmig et al. 2020). Since TR-AMs inhabit an environment with high oxygen levels, we hypothesized that TR-AMs may not be able to induce glycolytic reprogramming in response to either inflammatory stimuli or to physiologic hypoxia. Glycolysis stress tests were performed following overnight (16 hours) exposure to decreasing levels of ambient oxygen. Unlike their inability to induce glycolysis after inflammatory stimulus under normoxia, TR-AMs exhibited a progressive increase in the extracellular acidification rate (ECAR) in response to escalating degrees of ambient hypoxia (Figure 1A). Both basal rate of glycolysis and glycolytic reserve increased substantially when oxygen levels were lowered to 3.0% and 1.5% (Figure 1B). HIF-1 α levels were nearly undetectable under normoxic conditions; however, with increasing degrees of hypoxia, HIF-1 α stabilization occurred in a dose-dependent fashion and was detectable in the nucleus (Figure 1C) (Figure 1-source data 1 “*The effect of different O₂ concentrations on HIF1 α expression in TR-AMs.* Uncropped western blot images of HIF-1 α protein expression in TR-AMs under different concentrations of oxygen”). Pretreating TR-AMs prior to hypoxia with echinomycin, an inhibitor of HIF-1 α DNA binding activity (Kong, Park et al. 2005), disrupted hypoxia-induced increases in glycolytic rate in a dose-dependent fashion (Figure 1D). Echinomycin also reduced hypoxia-induced increases in glycolytic enzyme protein expression (HK2 and LDH), suggesting that HIF-1 α is required for glycolytic adaption to hypoxia in TR-AMs (Figure 1E) (Figure 1-source data 2 “*The effect of echinomycin on glycolytic enzyme protein expression in TR-AMs.* Uncropped western blot images of HK2, LDHA, and α -tubulin in TR-AMs treated with echinomycin under normoxia or hypoxia”). In concurrence with the echinomycin data, siRNA knockdown of HIF-1 α attenuated the hypoxia-induced increase in protein expression of

glycolytic enzymes and lactate production in TR-AMs (Figure 1-figure supplement 1A-C) (Figure 1-figure supplement 1-source data 1 “*Validation of Hif1a siRNA knockdown in TR-AMs*. Uncropped western blot images of HIF1 α protein expression in TR-AMs treated with either control siRNA or two different *Hif1a* siRNAs.” and Figure 1-figure supplement 1-source data 2 “*The effect of Hif1a siRNA knockdown on glycolytic enzyme protein expression in TR-AMs under normoxia and hypoxia*. Uncropped western blot images of HK2, LDHA and α -tubulin expression in TR-AMs treated with either control siRNA or two different *Hif1a* siRNAs under normoxia or hypoxia”).

Both short-term (2 hours) and prolonged (16 hours) exposure to hypoxia (1.5% O₂) led to significant increases in nuclear HIF-1 α protein levels in TR-AMs (Figure 1-figure supplement 2A) (Figure 1-figure supplement 2-source data 1 “*Expression HIF-1 α protein in TR-AMs at different time points following exposure to hypoxia*. Uncropped western blot images of HIF1 α protein expression in TR-AMs treated with hypoxia for 0, 2, or 16 hours or with DMOG”). Glycolysis stress tests demonstrated that short-term hypoxia treatment failed to induce significant alterations in glycolysis or glycolytic capacity in TR-AMs compared to prolonged hypoxia treatment suggesting that transcription and translation of glycolytic genes that are targets of HIF-1 α are required (Figure 1-figure supplement 2B,C). Taken together, these data indicate that TR-AM HIF-1 α stabilization in response to hypoxia is dose-dependent, and that prolonged hypoxia, but not short-term hypoxia exposure, leads to a functional glycolytic phenotype in TR-AMs.

BMDMs have limited metabolic adaptation to hypoxia

Several studies have examined the effects of hypoxia on BMDM metabolism; however, they focused heavily on transcriptional changes in glycolytic gene expression as opposed to functional changes in glycolysis (Bosco, Puppo et al. 2006, Roiniotis, Dinh et al. 2009, Delprat,

Tellier et al. 2020). We found that, unlike TR-AMs, BMDMs exposed to hypoxia (16 hours) exhibit minimal changes in glycolytic rate or glycolytic capacity (Figure 1F-G). Interestingly, we found that BMDMs have high basal levels of nuclear HIF-1 α protein under normoxic conditions and that HIF-1 α expression in BMDMs did not significantly change in response to hypoxia as low as 1.5% O₂ (Figure 1H) (Figure 1-source data 3 “*The effect of different O₂ concentrations on HIF1 α expression in BMDMs*. Uncropped western blot images of HIF-1 α protein expression in BMDMs under different concentrations of oxygen”). Echinomycin had a minimal effect on the glycolytic output of hypoxic BMDMs (Figure 1I). Likewise, neither hypoxia nor hypoxia in combination with echinomycin altered glycolytic enzyme protein expression (HK2 and LDHA) in BMDMs (Figure 1J) (Figure 1-source data 4 “*The effect of echinomycin on glycolytic enzyme protein expression in BMDMs*. Uncropped western blot images of HK2, LDHA, and α -tubulin in BMDMs treated with echinomycin under normoxia or hypoxia”). SiRNA knockdown of *Hif1a* also had no impact on glycolytic protein expression or lactate production in BMDMs (Figure 1-figure supplement 1D-F) (Figure 1-figure supplement 1-source data 3 “*Validation of Hif1a siRNA knockdown in BMDMs*. Uncropped western blot images of HIF1 α protein expression in BMDMs treated with either control siRNA or two different *Hif1a* siRNAs” and Figure 1-figure supplement 1-source data 4 “*The effect of Hif1a siRNA knockdown on glycolytic enzyme protein expression in BMDMs under normoxia and hypoxia*. Uncropped western blot images of HK2, LDHA and α -tubulin expression in BMDMs treated with either control siRNA or two different *Hif1a* siRNAs under normoxia or hypoxia”). Duration of hypoxia exposure (2h vs 16h) had no significant effect on HIF-1 α stabilization (Figure 1-figure supplement 2D) (Figure 1-figure supplement 2-source data 2 “*Expression HIF-1 α protein in BMDMs at different time points following exposure to hypoxia*. Uncropped western blot images of HIF1 α protein expression in BMDMs treated with hypoxia for 0, 2, or 16 hours or with DMOG”) or glycolysis (Figure 1-figure

supplement 2E,F) in BMDMs. Collectively, these data demonstrate that hypoxia has minimal effect on glycolytic function and HIF-1 α stabilization in BMDMs.

The hypoxia-induced transcriptomic response differs substantially between TR-AMs and BMDMs

To better understand the observed differences in hypoxia-induced glycolytic metabolism between TR-AMs and BMDMs, we performed RNA-sequencing to assess global alterations in gene expression. We found 741 DEGs (512 upregulated and 229 downregulated) in TR-AMs in response to 1.5% O₂ compared to only 260 DEGs (214 upregulated and 46 downregulated) in BMDMs (Figure 2A). Reactome pathway analysis revealed that hypoxia altered a large number of TR-AM genes in multiple pathways ranging from cellular metabolism, hemostasis, and immune cell function, while the majority of BMDM genes affected by hypoxia were related to carbohydrate metabolism (Figure 2B). Hypoxia led to the most significant increases in glycolytic and HIF-1 α regulatory gene expression in both TR-AMs and BMDMs. These same genes were significantly lower in TR-AMs compared to BMDMs under normoxic conditions (Figure 2C) (Figure 2-source data 1 *“Read count data for hypoxia-regulated genes in TR-AMs and BMDMs”*). This is in direct agreement with our previous findings (Woods, Kimmig et al. 2020). A side-by-side comparison demonstrated that the level of HIF-1 α expression in hypoxic TR-AMs is similar to that of BMDMs under normoxia and hypoxia (Figure 2D) (Figure 2-source data 2 *“Differences in HIF-1 α expression between TR-AMs and BMDMs under normoxia and hypoxia. Uncropped western blot images of HIF1 α expression in TR-AMs and BMDMs treated with normoxia or hypoxia”*). Hypoxia-induced HIF-1 α expression in TR-AMs correlated with increase in glycolytic (HK2 and LDHA) and prolyl hydroxylase (EGLN1 and EGLN3) protein expression in TR-AMs (Figure 2E) (Figure 2-source data 3 *“Differences in glycolytic enzyme and prolyl hydroxylase protein expression between TR-AMs and BMDMs under normoxia and hypoxia. Uncropped western blot images of HK2, LDHA, PHD2, PHD3 and α -tubulin expression in TR-*

AMs and BMDMs treated with normoxia or hypoxia”). This was not the case in BMDMs in which hypoxia exposure did not alter protein expression of glycolytic genes. These results demonstrate that hypoxia induces transcriptomic alterations in TR-AMs that lead to changes in protein expression and metabolic function. In contrast, BMDMs exhibit high levels of HIF-1 α and HIF-1 α target proteins at baseline, and do not further increase the expression of these proteins in response to hypoxia, despite a hypoxia-adaptive mRNA transcription (Figure 2D and 2E).

Hypoxia modulates TR-AM cytokine production and metabolic response to LPS

Hypoxia and HIF-1 α are thought to be central to the inflammatory response of macrophages (Cramer, Yamanishi et al. 2003, Tannahill, Curtis et al. 2013, Palsson-McDermott, Curtis et al. 2015). To determine the effect of HIF-1 α stabilization on TR-AM's effector response, we measured the production of proinflammatory cytokines in response to LPS under hypoxia. TR-AMs were exposed overnight to hypoxia (1.5% O₂) or normoxia and then subsequently treated with LPS while maintaining original O₂ conditions. Hypoxia alone did not stimulate cytokine production without LPS treatment. Hypoxic TR-AMs secreted significantly higher levels of TNF- α , KC, and IL-1 β in response to LPS compared to normoxic controls. In contrast, IL-6 and CCL2 secretion was decreased in hypoxic TR-AMs (Figure 3A). The cytokine gene expression pattern in hypoxic TR-AMs treated with LPS mirrored the secreted cytokine profile (Figure 3B). Moreover, enhanced proIL-1 β protein production was observed in hypoxic TR-AMs treated with LPS (Figure 3C) (Figure 3-source data 1 “*Changes in LPS-induced expression of proIL-1 β protein in TR-AMs under normoxia and hypoxia*. Uncropped western blot images of proIL-1 β protein in TR-AMs treated with LPS for 6 or 24 hours under normoxia or hypoxia”). While BMDMs experienced limited metabolic alterations in response to hypoxia, treatment with LPS revealed that hypoxia induced similar alterations in their cytokine profile. Hypoxic BMDMs had increased TNF- α , KC, and IL-1 β , and decreased IL-6 secretion (Figure 3-figure supplement 1). The only discordance in the hypoxic cytokine response profile between TR-AMs and BMDMs

was CCL2, which remained unchanged in hypoxic BMDMs in response to LPS compared to normoxic controls (Figure 3-figure supplement 1).

We and others have shown that BMDMs exhibit an immediate enhancement in glycolytic output in response to LPS (Figure 3-figure supplement 2). It is thought that this increase in glycolysis following LPS supports the proinflammatory response. We have shown that LPS-induced inflammation in TR-AMs is independent of glycolysis including the rise in glycolysis following LPS injection (Woods, Kimmig et al. 2020). Given that hypoxia elevated HIF-1 α levels and glycolytic rates in TR-AMs, we sought to determine if hypoxia could alter TR-AM glycolytic responsiveness to LPS. We found that despite the fact that hypoxia increased the glycolytic rate of TR-AMs at baseline, TR-AM glycolysis remained unresponsive to LPS injection (Figure 3D). Using capillary electrophoresis-mass spectrometry to measure glycolytic metabolite levels, we found that consistent with increased glycolytic output after hypoxia, levels of glycolytic intermediate metabolites (glucose-6 phosphate, fructose 1,6 diphosphate, glycerol 3-phosphate, dihydroxyacetone phosphate) and lactate were increased in response to hypoxia alone. Interestingly, hypoxic TR-AMs exhibited further increases in glycolytic intermediates in the presence of LPS (6h) compared to normoxic cells, suggesting that while LPS increases cellular levels of glycolytic metabolites in hypoxic TR-AMs, this does not manifest as acute lactate secretion (Figure 3E). These data demonstrate that hypoxia leads to significant alterations in TR-AM cytokine production and increased glycolytic metabolites in response to prolonged LPS treatment. However, unlike the prototypical BMDM response, hypoxic TR-AMs do not immediately increase their extracellular acidification in response to LPS.

We have previously shown that unlike BMDMs, TR-AMs effector function is acutely sensitive to mitochondrial inhibition (Woods, Kimmig et al. 2020). Since TR-AM capacity for glycolysis expands with decreasing levels of O₂, we next sought to assess mitochondrial function under

hypoxia and performed a mitochondrial stress test on TR-AMs that had been exposed to varying oxygen concentrations. Interestingly, mild-to-moderate degrees of ambient hypoxia did not appear to significantly alter overall mitochondrial function in these cells. Only 1.5% O₂ caused significant reductions in oxygen consumption rate (OCR) across all mitochondrial parameters (Figure 4A, B). ECAR tracings during the mitochondrial stress test demonstrated that, other than severe hypoxia (1.5% O₂), the majority of acid produced under mild-moderate hypoxia is derived from CO₂, as the application of rotenone and antimycin A led to a significant reduction in ECAR (Figure 4C). When exposed to 1.5% O₂, TR-AM energy is derived mostly from glycolysis with no significant contribution of mitochondrial-derived CO₂ to extracellular acidification. Overall BMDM mitochondrial function was impaired by 1.5% O₂, but the effect was greatly diminished compared to TR-AMs (Figure 4-figure supplement 1A,B). BMDM ECAR tracing during mitochondrial stress test demonstrated that most acid production remained unchanged in response to rotenone and antimycin A regardless of O₂ concentration (Figure 4-figure supplement 1C). This suggests that BMDM acidification is glycolytically-derived under both normoxia and hypoxia.

TR-AM cytokine production in response to LPS was highly susceptible to inhibition by low doses of ETC inhibitors, rotenone and antimycin A, under normoxic conditions. This effect was greatly attenuated after exposure to hypoxia (Figure 4D). Additionally, high doses of ETC inhibitors induce cytotoxicity in normoxic TR-AMs, but hypoxic preconditioning significantly enhanced TR-AM cell viability (Figure 4E). In contrast, BMDM cytokine production was only marginally affected by ETC inhibition with the exception of observed decrease in IL-1 β . Unlike TR-AMs, hypoxia did not significantly alter BMDM cytokine production in the presence of ETC inhibitors (Figure 4-figure supplement 1D). Similarly, ETC inhibition did not to induce cytotoxicity in BMDMs under normoxia or hypoxia (Figure 4-figure supplement 1E).

TR-AM survival correlates with a shift to glycolytic metabolism during influenza-induced acute lung injury

LPS is a well-known and potent macrophage activator that in isolation can be used to investigate essential immune functions, such as cytokine production, signal transduction, and immunometabolism. It induces a broad range of inflammatory effects in macrophages making it a convenient tool to study overall immune fitness *in vitro*. However, *in vivo* studies have shown that LPS instillation into the murine airway leads to an immune response predominated by infiltrating neutrophils making LPS-induced ALI an unsuitable model to study macrophages (Chignard and Balloy 2000). Compared to LPS, influenza infection is a more clinically relevant model of ARDS, and various macrophage populations play a larger role in both exacerbating and limiting lung injury in this model (Short, Kroeze et al. 2014). Several groups have demonstrated that TR-AMs undergo cell death in response to influenza infection and that depletion of TR-AMs is associated with worse outcomes in models of influenza-induced ALI (Kim, Lee et al. 2008, Jaworska, Coulombe et al. 2014, Nelson, Zhou et al. 2014, Schneider, Nobs et al. 2014, Cardani, Boulton et al. 2017). To confirm this phenomenon, we utilized PKH26 Red Fluorescent Linker dye to specifically label, track, and collect TR-AMs over the time course of infection as we and others have previously described (Maus, Herold et al. 2001, Maus, Grote et al. 2002, Woods, Kimmig et al. 2020). In agreement with Zhu et al. (Zhu, Wu et al. 2021), we found that there was a significant decrease in TR-AMs (PKH26+) at 3 (D3) and 6 (D6) days post infection along with a subsequent increase in infiltrating, monocyte-derived alveolar macrophages (Mo-AMs) (Figure 5A). From these experiments, we performed RNAseq on sorted TR-AMs (PKH26+) and Mo-AMs (PKH26-) at D0, D3, and D6 (note: Mo-AMs are not present in an uninfected (D0) mouse)) to identify changes in the metabolic gene signature of these two macrophage populations during influenza infection. From D0 to D6, RNAseq data revealed that TR-AMs experienced decreased expression in genes related to oxidative phosphorylation with simultaneous increased expression of genes related to glycolytic metabolism. Moreover, the

metabolic gene signature of D6 TR-AMs was most similar to that of Mo-AMs at D3 and D6 (Figure 5B, C) (Figure 5-source data 1 “*Read counts data for genes of oxidative phosphorylation in TR-AMs and Mo-AMs*” and Figure 5-source data 2 “*Read counts data for genes of glycolysis in TR-AMs and Mo-AMs*”). Taken together, these data suggest that influenza-induced ALI leads to a decrease in TR-AM number, and that the surviving TR-AMs’ gene signature shifts away from genes related to mitochondrial metabolism in favor of glycolysis.

HIF-1 α stabilization increases TR-AM survival and improves outcomes in influenza-induced acute lung injury

Given that the reduced TR-AM population on D6 presented with a glycolytic gene signature, we hypothesized that TR-AM survival was dependent upon a metabolic shift to glycolysis. In other words, a decrease in TR-AM numbers overtime was due to a large fraction of the cells failing to metabolically adapt to the conditions of the infected/hypoxic alveoli. Thus, TR-AMs that could not adapt to hypoxia and retained primarily mitochondria-driven metabolism died off while TR-AMs that shifted to glycolytic metabolism survived. To test this hypothesis, we first sought to determine if stabilization of HIF-1 α was sufficient to induce a hypoxic metabolic state in AMs without altering O₂ levels. To do this, we treated cells with FG-4592, an inhibitor of HIF prolyl hydroxylases. FG-4592 has a greater potency and fewer off target effects compared to DMOG, which broadly inhibits 2-oxoglutarate-dependent oxygenases (Singh, Wilson et al. 2020). TR-AMs treated with FG-4592 for 16 hours exhibited a significant dose-dependent increase in glycolysis. (Figure 6A, B). FG-4592 induced robust HIF-1 α stabilization leading to increased expression of HK2, LDHA, PHD1, and PHD3 (Figure 6C, D) (Figure 6-source data 1 “*The effect of FG-4592 on HIF-1 α expression in TR-AMs*. Uncropped western blot images of HIF1 α in TR-AMs treated with FG-4592 or control vehicle” and Figure 6-source data 2 “*The effect of FG-4592 on glycolytic enzyme and prolyl hydroxylase protein expression in TR-AMs*. Uncropped western blot images of HK2, LDHA, PHD2, PHD3 and α -tubulin in TR-AMs treated with FG-4592 or

control vehicle"). Unlike hypoxia (1.5% O₂), FG-4592 had very little impact on overall mitochondrial fitness in TR-AMs (Figure 6E). Basal respiration and mitochondrial ATP production were reduced, but spare mitochondrial compacity was increased, signaling a shift toward glycolytic ATP production at baseline but no loss in overall mitochondrial function (Figure 6E-G). Like hypoxia, FG-4592 treatment could also rescue ETC inhibitor-induced impairment in cytokine production (Figure 6H) and cell death in TR-AMs (Figure 6I). However, unlike TR-AMs exposed to 1.5% O₂, FG-4592 did not broadly alter LPS cytokine responses suggesting that changes in the cytokine profile under hypoxia are oxygen-dependent, but remain independent of HIF-1 α stabilization (Figure 6H).

We next treated mice intratracheally with one dose of FG-4592 at the time of infection to evaluate the effect of early glycolytic adaptation on TR-AM survival and influenza-induced acute lung injury. Strikingly, FG-4592 treatment resulted in increased TR-AM (PKH26+ cells) survival at 6 days post infection (dpi) compared to infected controls (Figure 7A). The increase in TR-AM survival in FG-4592-treated mice was associated with reduced alveolar permeability (Figure 7B). FG-4592 treatment also led to a reduction in pro-inflammatory cytokine levels within the alveolar space at 6dpi (Figure 7C). Most importantly, FG-4592 treated mice experienced reduced weight loss and improved survival compared to infected controls (Figure 7D, E). Taken together, these data suggest intratracheal FG-4592 treatment can increase TR-AM survival and improve outcomes in influenza-infected mice.

DISCUSSION

ARDS is associated with high morbidity and mortality. Despite many decades of research, treatment remains supportive and there is no therapy that directly targets the pathogenesis of ARDS. Infection is the main cause of ARDS. Respiratory viruses such as influenza A virus and SARS-CoV-2 cause significant mortality by causing ARDS. In fact, the 2009 influenza pandemic and the ongoing COVID19 pandemic have shown that acute respiratory illnesses can have a profound effect on society in the 21st Century. ARDS caused by influenza A and SARS-CoV-2 viruses is associated with loss of TR-AMs, that correlates with disease severity and mortality (Ghoneim, Thomas et al. 2013, Liao, Liu et al. 2020, Grant, Morales-Nebreda et al. 2021, Zhu, Wu et al. 2021). Because TR-AMs maintain a central role in lung homeostasis and response to airborne pathogens, understanding basic TR-AM processes, like metabolic adaptation in response to an altered lung environment during acute lung injury/ARDS, may allow us to therapeutically rescue TR-AM cell death, and augment their function to improve outcomes in acute respiratory illnesses.

We have previously demonstrated that TR-AMs are remarkably adapted to the high oxygen, low glucose environment of the alveolar lumen and do not require glucose or glycolysis to carry out their effector function as monocyte-derived macrophages do (Woods, Kimmig et al. 2020). ARDS leads to significant hypoxia to which TR-AMs need to adapt; thus, we sought to determine whether TR-AMs displayed metabolic plasticity during conditions of low oxygen. In this study, we found that TR-AMs adapted to hypoxia through HIF-1 α induction. Hypoxia stabilized TR-AM HIF-1 α in a dose-dependent manner resulting in robust increases in glycolytic protein expression and function. These changes were dependent on HIF-1 α , as hypoxic TR-AMs treated with echinomycin, an inhibitor of HIF-1 α DNA binding activity, lost their glycolytic capabilities. In contrast, BMDMs exhibited robust HIF-1 α stabilization under normoxic conditions and BMDM HIF-1 α expression and glycolytic output remained unchanged in response to

hypoxia. Transcriptomic analysis found 741 DEGs in TR-AMs in response to hypoxia compared to only 260 DEGs in BMDMs. This differential sensitivity to hypoxia observed in TR-AMs and BMDMs is likely tied to differences in developmental processes and respective, local tissue environments (Hussell and Bell 2014, Bain and MacDonald 2022). TR-AMs are derived from embryonic progenitors (fetal monocytes) and mature upon lung localization during development (Guilliams, De Kleer et al. 2013). Under steady-state conditions, the high oxygen, low glucose environment of the alveolar lumen favors a cell type that relies on oxygen-based metabolism making glycolysis an inefficient means to fuel cellular processes. The transcriptional signature of TR-AMs is enriched with genes associated with lipid metabolism (Gibbings, Goyal et al. 2015, Leach, Gibbings et al. 2020). The alveolar lumen contains an abundance of fatty acid molecules in the form of pulmonary surfactant. TR-AMs are critical in recycling surfactant in the healthy airway (Whitsett, Wert et al. 2010). While the TR-AMs' preferred steady-state mitochondrial fuel remains elusive, it is likely that they utilize fatty acids for energy by catabolizing pulmonary surfactant. ARDS leads to hypoxia accompanied by an influx of glucose and dramatic decreases in pulmonary surfactant molecules (Hofer, Woods et al. 2015, Woods, Doolittle et al. 2016, Schousboe, Ronit et al. 2022). This suggests that TR-AMs would need to significantly augment their metabolism to survive, and likely explains why HIF1 α induction in TR-AMs is so sensitive to hypoxia and why RNAseq analysis revealed a much greater number of hypoxia response genes in TR-AMs compared to BMDMs. In contrast, BMDMs/monocytes are derived from adult hematopoietic stem cells and arise from the bone marrow where oxygen concentrations vary from 1.5-4% (Spencer, Ferraro et al. 2014). BMDMs/monocytes circulate in the blood and traffic to sites of inflammation, which both have significantly higher glucose levels compared to the steady-state alveoli. These conditions favor constitutive expression of HIF1 α and necessitate a functional glycolytic phenotype to fuel cellular processes. Thus, macrophage/monocyte populations arising from the bone-marrow, where hypoxic conditions are observed under steady-state conditions, are likely less-sensitive to hypoxia stimulus *in vitro*.

Indeed, our *in vivo* experiments show that although TR-AMs are lost during ARDS, the surviving TR-AMs are glycolytically adapted and resemble recruited macrophages in metabolic gene expression. This is consistent with our previous findings that TR-AM viability is exquisitely sensitive to mitochondrial inhibition while BMDM viability is unaffected. Our current findings show that hypoxia restores viability to TR-AMs under mitochondrial inhibition and reverses the suppressive effects of this inhibition on TR-AM cytokine production supporting optimal effector function in a low oxygen environment. These data suggest that the link between immune effector function and metabolism in TR-AMs is based on overall cellular fitness, and that the environmental shift from high oxygen and low glucose under steady-conditions to low oxygen and increased glucose during lung injury may necessitate cellular adaptation to the microenvironment to ensure survival.

While we are unable to directly measure the alveolar oxygen concentration during lung injury, several lines of evidence provide justification for the use of oxygen levels as low as 1.5% O₂ for our *in vitro* studies. Severe hypoxia is observed in the airways in both chronic and acute lung disease (Schaible, Schaffer et al. 2010). For example, bronchoscopy measurements in CF patients recorded O₂ levels below 1% in mucopurulent bronchi (Worlitzsch, Tarran et al. 2002). Murine influenza infection yields a rapid decline in alveolar gas exchange in a manner that models human ARDS (Wolk, Lazarowski et al. 2008, Traylor, Aeffner et al. 2013). These observations correlate with impaired alveolar fluid clearance, interstitial edema, alveolar damage, and inflammatory infiltrates that all likely limit oxygen diffusion into the alveolar space (Aeffner, Bolon et al. 2015). In ARDS, cells such as TR-AMs residing in the areas of lungs that are filled with protein rich fluid and those with complete atelectasis are potentially subjected to severe hypoxia and even anoxia. Xi et al used piminidazole to identify hypoxic alveoli during influenza infection (Xi, Kim et al. 2017). While piminidazole cannot provide quantitative measurements in relation to oxygen concentrations, biochemical analysis suggests that 2-

nitroimidazole compounds label cells once O₂ levels drop to approximately 1.3% O₂ (Gross, Karbach et al. 1995). Taken together, these observations suggest that the alveolar space can become severely hypoxic during influenza-induced lung injury.

Pharmacological depletion of TR-AMs has offered insight into their beneficial immunoregulatory properties in various lung injury models. TR-AMs have been shown to alleviate lung injury by clearing apoptotic neutrophils, suppressing T-cell-mediated inflammatory responses, and limiting dendritic cell infiltration and antigen presentation (Thepen, Van Rooijen et al. 1989, Holt, Oliver et al. 1993, Knapp, Leemans et al. 2003, Jakubzick, Tacke et al. 2006). Loss of TR-AMs during influenza infection is known to enhance mortality, and several studies have shown that there is a progressive loss of TR-AMs over the time course of infection (Kim, Lee et al. 2008, Ghoneim, Thomas et al. 2013, Schneider, Nobs et al. 2014, Cardani, Boulton et al. 2017, Zhu, Wu et al. 2021). Why TR-AMs are lost during the course of IAV infection is not understood. We hypothesized that failure to adapt to the hypoxic environment may play a role in the TR-AM loss. We found that HIF-1 α activation was sufficient to promote glycolysis, and rescue TR-AM viability and effector function under mitochondrial inhibition. Furthermore, when mice were treated with a HIF-1 α stabilizer at the time of influenza infection, TR-AM survival was increased, and accompanied by reduced lung injury and death. These findings suggest that HIF-1 α is essential for TR-AM cell survival, and that increasing TR-AM cell number by promoting their adaptation to ARDS associated changes in the microenvironment during infection reduces lung injury.

In agreement with our findings, Zhu and colleagues recently showed that TR-AMs at D6 of influenza infection have high HIF-1 α expression; however, they suggested that HIF-1 α stabilization in TR-AMs worsens lung injury through enhanced proinflammatory effector function (Zhu, Wu et al. 2021). This study relied on the use of a non-inducible *Cd11c* cre allele to knockout HIF-1 α in TR-AMs. While TR-AMs do express high levels of *Cd11c*, this marker is not

specific for TR-AMs, and is also expressed in different monocyte/macrophage populations, dendritic cells, and natural killer cells (Abram, Roberge et al. 2014). Moreover, as monocyte-derived macrophages enter the alveolar space, they begin to express Cd11c (Misharin, Morales-Nebreda et al. 2013). Thus, it cannot be determined from these experiments whether the observed effect of HIF-1 α deletion on inflammation and lung injury was specific for TR-AMs as the recruited monocyte-derived macrophages will also lose HIF-1 α as they enter the lungs. It is likely that the recruitment of monocyte-derived macrophages was inhibited by HIF-1 α deletion, resulting in reduced inflammation and lung injury (Cramer, Yamanishi et al. 2003). Using FG-4592 *in vitro*, we found that HIF-1 α stabilization and glycolytic reprogramming resulted in no significant changes in proinflammatory cytokine production downstream of LPS. Furthermore, we show that treatment of mice with FG-4592 promoted survival of TR-AMs after influenza infection, and lead to reduced levels of lung injury. While intratracheal FG-4592 installation improved outcomes in influenza-infected mice, we cannot definitively say that the beneficial effects are solely related to HIF-1 α induction in TR-AMs since our delivery strategy could also affect lung epithelial cells, which might indirectly contribute to the results. Methodologies allowing for TR-AM specific delivery of FG-4592 would resolve this issue. Alternatively, a genetic approach allowing for inducible HIF-1 α activation could conclusively demonstrate whether HIF-1 α expression specifically in TR-AMs promotes survival during lung injury since constitutive expression of HIF-1 α leads to defects in TR-AM development (Izquierdo, Brandi et al. 2018). There have also been no studies on the effects of long-term HIF-1 α activation and resultant metabolic reprogramming in TR-AMs under steady state or during recovery from inflammatory stimuli. Thus, our short-term pharmacologic activation of HIF-1 α and glycolytic reprogramming in TR-AMs is a useful model for studying the role of metabolic reprogramming during lung injury.

512 Interestingly, we found that the effects of hypoxia on both TR-AM and BMDM effector function
513 appears to be independent of HIF-1 α . While HIF-1 α stabilization was sufficient to drive
514 metabolic reprogramming in TR-AMs, FG-4592 did not affect cytokine production downstream
515 of LPS. By contrast, when cultured in hypoxia TR-AMs exhibited marked changes in their
516 secreted cytokine profile including increased secretion of TNF- α , KC, and IL-1 β and less IL-6
517 and CCL2 compared to normoxic controls. BMDMs exposed to hypoxia and treated with LPS
518 responded similarly to TR-AMs with the exception to CCL2, which remained unchanged in
519 response to hypoxia in BMDMs. This was independent of any effect of hypoxia on HIF-1 α
520 stabilization or target gene expression in BMDMs. Similarities between TR-AMs and BMDMs in
521 terms of cytokine profiles would suggest that low oxygen concentrations may be driving these
522 changes independently of HIF-1 α stabilization. Further investigation will be required to elucidate
523 the mechanisms by which a low oxygen environment alters cytokine production.

524
525 In conclusion, under normoxic conditions, TR-AMs depend on mitochondrial respiration,
526 inhibition of which leads to decreased effector response and cell death. Under hypoxic
527 conditions, as occurs during ARDS, TR-AMs stabilize HIF-1 α in a dose dependent manner and
528 have a robust HIF-1 α response compared to BMDMs. Stabilization of HIF-1 α allows TR-AMs to
529 augment glycolytic function, and prevents their death following the inhibition of mitochondrial
530 respiration as well as following influenza A viral infection. These data suggest that therapies
531 inducing HIF-1 α in TR-AMs may be beneficial in ARDS by preventing their death through
532 metabolic adaptation to the ARDS microenvironment that is low in O₂ and high in glucose.

Key Resources Table				
Reagent type (species) or resource	Designation	Source or reference	Identifiers	Additional information
Strain, strain background (M. musculus)	C57BL/6J	Jackson Laboratory	Stock No. 000664	6-8 weeks
Strain, strain background (Influenza A virus)	A/PR8/34 (H1N1)	BEI Resources, NIAID, NIH	NR-348	
Antibody	Anti-HK2 (rabbit monoclonal)	Cell Signaling Technology	Catalog #: C64G5	WB (1:1000)
Antibody	Anti-LDHA (rabbit polyclonal)	Cell Signaling Technology	Catalog #: 2012S	WB (1:1000)
Antibody	Anti-PHD2/EGLN1 (rabbit monoclonal)	Cell Signaling Technology	Catalog #: 4835	WB (1:1000)
Antibody	Anti-PHD3/EGLN3 (rabbit polyclonal)	Novus Biologicals	Catalog #: NB100-303	WB (1:1000)
Antibody	Anti-IL-1 β (mouse monoclonal)	Cell Signaling Technology	Catalog #: 12242	WB (1:1000)
Antibody	Anti-Lamin B1 (rabbit polyclonal)	Proteintech	Catalog #: 12987-1-AP	WB (1:1000)
Antibody	Anti-HIF-1 α (rabbit polyclonal)	Cayman Chemical	Catalog #: 10006421	WB (1:500)
Antibody	Anti- α -Tubulin (mouse monoclonal)	Sigma	Catalog #: T6074	WB (1:20000)
Antibody	Anti-rabbit IgG,	Cell Signaling	Catalog #:	WB (1:2500)

	HRP-linked Antibody (goat polyclonal)	Technology	7074	
Antibody	Anti-mouse IgG, HRP-linked Antibody (horse polyclonal)	Cell Signaling Technology	Catalog #: 7076	WB (1:2500)
Antibody	CD16/CD32 (FcBlock) (rat monoclonal)	BD Biosciences	Clone 2.4G2; Catalog #: 553141	Flow Cytometry (1:50)
Antibody	AlexaFluor 700 anti-mouse Ly-6G (rat monoclonal)	BioLegend	Clone 1A8; Catalog #: 553141	Flow Cytometry (1:250)
Chemical compound, drug	FG-4592 (Roxadustat)	Cayman Chemical	Catalog #: 15294	
Chemical compound, drug	Recombinant Mouse M-CSF	BioLegend	576406	
Chemical compound, drug	Oligomycin	Fisher Scientific	49-545-510MG	
Chemical compound, drug	FCCP	Millipore Sigma	C2920	
Chemical compound, drug	Antimycin A	Millipore Sigma	A8674	
Chemical compound, drug	Rotenone	Millipore Sigma	R8875	
Chemical compound, drug	Lipopolysaccharide	Santa Cruz	sc-3535	
Commercial assay or kit	Mouse IL-6 DuoSet ELISA	R and D Systems	DY406	

Commercial assay or kit	Mouse TNF- α DuoSet ELISA	R and D Systems	DY410	
Commercial assay or kit	Mouse KC DuoSet ELISA	R and D Systems	DY453	
Commercial assay or kit	Mouse CCL2 DuoSet ELISA	R and D Systems	DY479	
Commercial assay or kit	Mouse IL-1 β alpha DuoSet ELISA	R and D Systems	DY401	
Commercial assay or kit	Lactate Assay Kit	Millipore Sigma	MAK064-1KT	
Commercial assay or kit	Mouse Macrophage Nucleofector Kit	Lonza	VPA-1009	
Commercial assay or kit	Seahorse XFe24 FluxPak	Agilent	102340–100	
Commercial assay or kit	NE-PER Nuclear and Cytoplasmic Extraction Reagents	ThermoFisher	Catalog #:78833	
Other	PKH26 Cell Linker Dye for Phagocytic Cell Labeling	Millipore Sigma	Cat. #: PKH26PCL-1KT	Dye to distinguish between TR-AMs and Mo-AMs
Other	SYTOX Green Nucleic Acid Stain	ThermoFisher	Catalog #: S7020	Stain to distinguish between live and dead cells.
Sequence-based reagent	<i>Rpl19_F</i>	This paper	PCR Primers	CCGACGAAAGG GTATGCTCA
Sequence-based reagent	<i>Rpl19_R</i>	This paper	PCR Primers	GACCTTCTTTTT CCCGCAGC
Sequence-based reagent	<i>Il6_F</i>	This paper	PCR Primers	TTCCATCCAGTT GCCTTCTTGG
Sequence-based reagent	<i>Il6_R</i>	This paper	PCR Primers	TTCCTATTTCCA CGATTTCCCAG
Sequence-	<i>Tnfa_F</i>	This paper	PCR Primers	AGGGGATTATG

based reagent				GCTCAGGGT
Sequence-based reagent	<i>Tnfa_R</i>	This paper	PCR Primers	CCACAGTCCAG GTCAGTGC
Sequence-based reagent	<i>Il1b_F</i>	This paper	PCR Primers	GCCACCTTTTGA CAGTGATGAG
Sequence-based reagent	<i>Il1b_R</i>	This paper	PCR Primers	GACAGCCCAGG TCAAAGGTT
Sequence-based reagent	<i>Kc_F</i>	This paper	PCR Primers	AGACCATGGCT GGGATTCAC
Sequence-based reagent	<i>Kc_R</i>	This paper	PCR Primers	ATGGTGGCTAT GACTTCGGT
Sequence-based reagent	<i>Ccl2_F</i>	This paper	PCR Primers	CTGTAGTTTTTG TCACCAAGCTCA
Sequence-based reagent	<i>Ccl2_R</i>	This paper	PCR Primers	GTGCTGAAGAC CTTAGCCCA
Sequence-based reagent	Non-targeting (control) siRNA	Dharmacon	D-001810-01	
Sequence-based reagent	<i>Hif1a</i> #1; J-040638-06	Dharmacon	J-040638-06	
Sequence-based reagent	<i>Hif1a</i> #2; J-040638-07	Dharmacon	J-040638-07	
Software, algorithm	FastQC	Babraham Institute	RRID: SCR_014583	
Software, algorithm	STAR	PMID: 23104886	RRID: SCR_015899	
Software, algorithm	DESeq2	Bioconductor	RRID: SCR_015687	
Software, algorithm	Reactome Cytoscape Plugin	PMID: 14597658	RRID: SCR_003032	
Software, algorithm	Prism 9	GraphPad	RRID: SCR_002798	

534

535

Primary Culture of Macrophages

All animal experiments and procedures were performed according to the protocols (ACUP7236 and ACUP72484) approved by the Institutional Animal Care and Use Committee at the University of Chicago. 6-8 week old C57BL/6 mice were humanely euthanized, and their TR-AMs were isolated via standard bronchoalveolar lavage (intratracheal instillation) using PBS + 0.5 mM EDTA. Following isolation, TR-AMs were counted, plated in RPMI 1640 (ThermoFisher, catalog number 11875119) supplemented with 10% FBS (Gemini, catalog number 100-106) and 1% penicillin-streptomycin (Gemini, catalog number 400-109), and allowed to adhere to tissue culture plates for one hour prior to experimentation. BMDMs were generated by isolating bone marrow cells from the femur and tibia bones of 6-8 week old C57BL/6 mice. Bone marrow cells were differentiated into BMDMs using 40 ng/mL recombinant M-CSF (BioLegend, catalog number 576406) in the same media formulation as TR-AMs. On day seven, BMDMs were replated and allowed to adhere to tissue culture plates for two hours prior to experimentation. After adherence, cells were washed, fresh media added, and placed under experimental conditions. For inflammatory stimulation, LPS was used at a concentration of 20ng/ml. For hypoxia experiments, macrophage cultures were placed in an airtight incubator system that utilizes N₂ displacement of O₂ to achieve hypoxic conditions (Coy Hypoxic Chamber- O₂ Control InVitro Glove Box). The sealed system ensures minimal fluctuations in O₂ levels in experiments when treating cultures and collecting samples under hypoxic conditions.

Bioenergetic Measurements

Glycolytic and mitochondrial respiration rates were measured using the XFe24 Extracellular Flux Analyzer (Agilent, Santa Clara, MA). BMDMs and TR-AMs were seeded at 4.0×10^4 /well onto Seahorse XF24 Cell Culture Microplates. Cells were equilibrated with XF Base media (Agilent, catalog number 103334-100) at 37 °C for 30 minutes in the absence of CO₂. Glycolytic rate was assessed using the manufacturers' protocol for the Seahorse XF Glycolysis Stress Test followed by sequential injections with glucose (10mM), oligomycin (1.0μM), and 2-DG

(100mM). Mitochondrial respiration rate was measured using the Seahorse XF Mito Stress Test according to the manufacturer's protocol followed by sequential injections with oligomycin (1.0 μ M), FCCP (1.0 μ M for BMDMs and 4.0 μ M for TR-AMs), and rotenone/antimycin A (1.0 μ M). Assessment of real-time metabolic responses to LPS was performed using the protocol detailed in an application note provided by the Agilent (Kam Y 2017). In brief, following plating, cells were equilibrated in XF base media supplemented with 10 mM glucose, 2 mM L-glutamine, 1 mM sodium pyruvate (Sigma, catalog number 11360070) and 5 mM HEPES (Sigma, catalog number 15630080), pH 7.4 and incubated at 37 °C without CO₂ for 30 minutes prior to XF assay. Baseline metabolic rates were measured followed by direct injection of LPS (final concentration:20ng/ml). Bioenergetic rates were subsequently measured every three minutes for approximately 5 hours in total.

Due to the limitations of the XFe24 Extracellular Flux Analyzer, all bioenergetic analysis on hypoxic samples was performed in the following manner. Cells were treated under hypoxic conditions (most commonly for 16 hours) then bioenergetic analysis was performed under normoxic conditions. Moreover, it is impossible to evaluate varying levels of hypoxia on a single Seahorse microplate. Thus, energy curves comparing varying levels of O₂ (i.e., Figure 1A) were performed individually and then subsequently represented on the same graph for comparison. All individual experiments were repeated a minimum of three times to ensure accurate representation and statistical comparison.

Cell lysis, subcellular fractionalization and Immunoblotting

Whole cell lysates were prepared by scraping cells into lysis buffer containing 25mM Tris HCl (pH 7.6), 150mM NaCl, 1% NP-40, 1% sodium deoxycholate, 0.1% SDS, 0.1% Benzonase, and Halt™ Protease Inhibitor Cocktail (ThermoFisher, catalog number 1861284 and 78430). Samples were centrifuged at 16,000 x g at 4 °C for 5 min to pellet cellular debris. Subcellular fractionalization and lysate preparation were carried out using the NE-PER Nuclear and Cytoplasmic Extraction Reagents (ThermoFisher, catalog number 78833). Lysate protein

concentration was determined using the Pierce™ BCA Protein Assay Kit (ThermoFisher, catalog number 23225). Equal concentrations of samples (15µg for whole cell lysates and 5µg for nuclear fractions) were resolved on Criterion gels (Bio-Rad, catalog number 5671093 and 5671094) and transferred to nitrocellulose (Bio-Rad, catalog number 1620167). Primary antibodies used were rabbit anti-HK2 (Cell signaling, catalog number C64G5, 1:1000), rabbit anti-LDHA (Cell signaling, catalog number 2012, 1:1000), rabbit anti-PHD2/Egln1 (Cell Signaling, catalog number 4835, 1:1000), rabbit anti-Egln3/PHD3 (Novus Biologicals, catalog number NB100-303, 1:1000), mouse anti-IL1β (Cell signaling, catalog number 12242 1:1000), rabbit anti-Lamin B1 (Proteintech, catalog number 12987-1-AP, 1:1000), rabbit anti-HIF-1α (Cayman Chemical, catalog number 10006421, 1:500), and mouse anti-tubulin (Sigma, catalog number T6074, 1:20,000). Secondary antibodies used were anti-rabbit IgG HRP-linked antibody (Cell Signaling, catalog number 7074, 1:2,500) and goat anti-mouse IgG HRP-linked antibody (Cell Signaling, catalog number 7076, 1:2,500). Protein expression was visualized using Immobilon ECL Ultra Western HRP Substrate (Millipore Sigma, catalog number WBULS0500) in combination with the BioRad ChemiDoc Touch Imaging system. All immunoblot data were repeated in at least three independent experiments.

Quantitative PCR

RNA was isolated from cells using the Direct-zol RNA MiniPrep kit (Zymo Research, catalog number R2052) and reverse transcribed using iScript Reverse Transcription Supermix (Bio-Rad, catalog number 1708841). Quantitative mRNA expression was determined by real-time qRT-PCR using iTaq Universal SYBR Green Supermix (Bio-Rad, catalog number 172-5121). *rlp19* served as a housekeeping gene, and gene expression was quantified using the $\Delta\Delta\text{ct}$ method to determine relative fold-change. The following mouse-specific primer sequences were used: *Rlp19* (5'-CCGACGAAAGGGTATGCTCA-3', 5'-GACCTTCTTTTCCCGCAGC-3'), *Ilf6* (5'-TTCCATCCAGTTGCCTTCTTGG-3', 5'-TTCCTATTTCCACGATTTCCCAG-3'), *Tnfa* (5'-

613 AGGGGATTATGGCTCAGGGT-3', 5'-CCACAGTCCAGGTCACTGTC-3', *Il1b* (5'-
614 GCCACCTTTTGACAGTGATGAG, 5'-GACAGCCCAGGTCAAAGGTT-3'), *Kc* (5'-
615 AGACCATGGCTGGGATTACAC-3', 5'-ATGGTGGCTATGACTTCGGT-3'), *Ccl2* (5'-
616 CTGTAGTTTTTGTCAACCAAGCTCA-3', 5'-GTGCTGAAGACCTTAGCCCA-3').

617 ***RNA-Sequencing***

618 RNA was isolated and submitted to the University of Chicago Genomics Core Facility for
619 sequencing with the Illumina NovaSEQ6000 sequencer (100bp paired-end). Sequencing read
620 (FASTQ) files were generated and assessed for per base sequence quality using FastQC.
621 Reads were mapped to the mouse genome (GRCm38.p6, GENCODE) using Spliced
622 Transcripts Alignment to a Reference (STAR) software, and the resulting gene transcripts were
623 quantified using featureCounts.

624 Gene counts were then imported into R for differential expression analysis using the
625 Bioconductor package DESeq2. Gene counts were filtered to remove low-expressing genes at a
626 threshold of 2 counts per million. Differential expression was calculated between normoxia and
627 hypoxia groups for both AMs and BMDMs. Differential gene expression was considered
628 significant for genes with an FDR-adjusted p-value < 0.05 and fold change (FC) > 2. Reactome
629 enrichment hit pathways and the linked gene lists from significant DEGs were identified by using
630 Reactome Cytoscape Plugin (Shannon, Markiel et al. 2003, Wu, Feng et al. 2010). Oxidative
631 phosphorylation and glycolysis gene sets were extracted from UniProtKB, then their associated
632 DEG read counts (TPM) were normalized using gensvm R package gensvm.maxabs.scale
633 function and center scaled for heat map visualization. All heatmaps were generated with Pretty
634 heatmaps R package pheatmap function.

635 ***Cytokine Analysis***

636 Secreted TNF α , IL-6, KC, CCL2, and IL-1 β levels were evaluated in macrophage media using a
637 standard sandwich ELISA (R&D Systems DuoSet ELISA Development System, catalog
638 numbers DY410, DY406, DY453, DY479 and DY401). For IL-1 β sample collection, 5mM ATP

was added to TR-AM cultures for 30 minutes following 6h LPS treatment to activate caspase 1, ensuring proIL-1 β cleavage and IL-1 β release. Rotenone and Antimycin A concentrations were 20nM for TR-AMs and 1 μ M for BMDMs when used in ELISA experiments.

Metabolomics

TR-AMs were plated at 2.5×10^6 on 60 mm plates for metabolite extraction. Following treatment, cells were washed twice with a 5% mannitol solution and metabolites were extracted using 400 μ l 100% methanol. 275 μ l of aqueous internal standard solution was mixed in with the methanol and the extract solution was transferred to a microcentrifuge. The extracts underwent centrifugation at $2,300 \times g$ at 4 °C for 5 min to precipitate insoluble material and the resulting supernatant was transferred to centrifugal filter units (Human Metabolome Technologies (HMT), Boston, MA). Filtering of supernatant occurred at $9,100 \times g$ at 4 °C for 2 hours. The filtrate was sent to HMT and analyzed using capillary electrophoresis–mass spectrometry.

Sulforhodamine B (SRB) Colorimetric Assay

In vitro cytotoxicity was measured using the SRB assay (Vichai and Kirtikara 2006). Following treatment, cells were fixed in 10% TCA and then stained with SRB dye. Cellular protein-dye complexes were solubilized in 10mM Tris base and the samples were read at OD 510 using a microplate reader. Data was normalized to the untreated, normoxia groups, which were representative of no cellular damage. ETC inhibitor concentration in BMDMs were as follows: 1 μ M rotenone, and 1 μ M antimycin A. ETC inhibitor concentration in TR-AMs were as follows: 500nM rotenone, and 100nM antimycin A.

SiRNA Knockdown

SiRNA knockdown was performed using the Amaxa™ Mouse Macrophage Nucleofector Kit (Lonzo, catalog number VPA-1009). 1.0×10^6 cells/reaction were resuspended in transfection solution with siRNA of interest (Dharmacon, Non-Targeting Control siRNA: D-001810-01; Mouse *Hif1a* siRNA #1; J-040638-06; Mouse *Hif1a* siRNA #2; J-040638-07). The cell solution

was then subjected to electroporation (Lonza Nucleofector 2b Electroporator: Setting Y-001). Cells were plated and allowed to rest for 6 hours then subjected to normoxia or hypoxia for 16 hours.

Lactate Assay

Secreted lactate was measured using the lactate colorimetric assay kit (Sigma, catalog number MAK064-1KT). Cells cultured in serum-free DMEM media (RPMI media and serum interfere with assay) and exposed to normoxia or 1.5% O₂. Samples were collected at 16 hours post treatment and manufacturer's protocol was followed to measure lactate.

Murine Influenza infection protocol and Survival Studies

C57BL/6 mice (6–8 weeks old) were anesthetized and challenged intratracheally (IT) with mouse-adapted influenza (A/PR8/34; 200 plaque-forming units [pfu]). A single FG-4592 (50uM) treatment was administered (IT) simultaneously with IAV. Body weight and survival was monitored every 24 hours for 20 days (10 mice/group). Body weight is represented as percent deviation from baseline at time of infection. "Influenza A virus, A/PR8/34 (H1N1), NR-348" was obtained through BEI Resources, NIAID, NIH.

BALF analysis

C57BL/6 mice were euthanized and a single 0.5ml saline wash was instilled into the lungs via the trachea and subsequently collected. BALF protein concentration was determined using the Pierce™ BCA Protein Assay Kit (ThermoFisher, catalog number 23225). BALF TNF α , IL-6, and IL-1 β were measured using sandwich ELISA.

Flow Cytometry

C57BL/6 mice (6–8 weeks old) were anesthetized with isoflurane and underwent retro-orbital injection with 100 μ l PKH26 Red Fluorescent Cell Linker Dye for Phagocytic Cell Labeling (catalog number PKH26PCL-1KT; Millipore Sigma) 1 day before lung challenge. The mice were then challenged intratracheally with IAV 100 (pfu). FG-4592 (50 μ M) was administered

intratracheally at the same time of PR8 infection. After challenge, the mice were euthanized and immune cells were collected via BAL. BAL cells were first treated with Fc Block (clone 2.4G2, catalog number 553141; BD Biosciences) and stained with fluorochrome-conjugated antibodies. The antibodies used were AlexaFluor 700 anti-mouse Ly-6G (Clone 1A8, catalog number 127621, 1:250; BioLegend). Immediately before sorting, cells were resuspended in sorting buffer (0.2% BSA in PBS) containing 5 nM SYTOX Green Nucleic Acid Stain (catalog number S7020; ThermoFisher) to distinguish between live and dead cells. Cell sorting was performed on a FACS Aria II instrument and data were acquired using BDFACS Diva software and analyzed with FCS Express 7 software. First, debris, red blood cells, and lymphocytes were eliminated based on size (FSC) and granularity (SSC). Next gates selected for live cells (FITC⁻) and eliminated neutrophils (Ly6G⁺). Based on previous validation experiments, the remaining cells are of macrophage lineage with TR-AMs being PKH26⁺ (SiglecF⁺, F4/80⁺, Cd11c^{Hi}, Ly6c^{Lo}) and Mo-AMs being PKH26⁻ (F4/80⁺, Cd11c^{Lo}, Ly6c^{Hi}). PKH26⁺ and PKH26⁻ cells were sorted into RNA lysis buffer and samples were prepared for RNAseq.

Statistics

The data were analyzed in Prism 9 (GraphPad Software Inc.). All data are shown as mean \pm standard deviation (SD). Significance was determined by unpaired, two-tailed Student's t test for comparisons between two samples, or by ANOVA using Bonferroni correction for multiple comparisons. P values <0.05 were considered statistically significant.

709 **ACKNOWLEDGEMENTS**

710 **Funding:** T32HL007605 (PSW, LMK, ORS, GMM), R01HL151680 (RBH) and R01ES010524,
711 U01ES026718, P01HL144454, and Department of Defense W81XWH-16-1-0711 (GMM).

712

713 **COMPETING INTERESTS**

714 PSW, RBH and GMM have a pending patent application (ARCD.P0740US.P1/1001176943) on
715 targeting tissue-resident alveolar macrophage metabolism to prevent their death during ARDS.
716 Otherwise, the authors do not have any competing interests.

REFERENCES

- Abram, C. L., G. L. Roberge, Y. Hu and C. A. Lowell (2014). "Comparative analysis of the efficiency and specificity of myeloid-Cre deleting strains using ROSA-EYFP reporter mice." Journal of immunological methods 408: 89-100.
- Aeffner, F., B. Bolon and I. C. Davis (2015). "Mouse Models of Acute Respiratory Distress Syndrome: A Review of Analytical Approaches, Pathologic Features, and Common Measurements." Toxicol Pathol 43(8): 1074-1092.
- Bain, C. C. and A. S. MacDonald (2022). "The impact of the lung environment on macrophage development, activation and function: diversity in the face of adversity." Mucosal Immunol 15(2): 223-234.
- Baker, E. H. and D. L. Baines (2018). "Airway Glucose Homeostasis: A New Target in the Prevention and Treatment of Pulmonary Infection." Chest 153(2): 507-514.
- Baker, E. H., N. Clark, A. L. Brennan, D. A. Fisher, K. M. Gyi, M. E. Hodson, B. J. Philips, D. L. Baines and D. M. Wood (2007). "Hyperglycemia and cystic fibrosis alter respiratory fluid glucose concentrations estimated by breath condensate analysis." Journal of Applied Physiology 102(5): 1969-1975.
- Beck-Schimmer, B., R. Schwendener, T. Pasch, L. Reyes, C. Booy and R. C. Schimmer (2005). "Alveolar macrophages regulate neutrophil recruitment in endotoxin-induced lung injury." Respiratory research 6(1): 61-61.
- Bosco, M. C., M. Puppo, C. Santangelo, L. Anfosso, U. Pfeffer, P. Fardin, F. Battaglia and L. Varesio (2006). "Hypoxia Modifies the Transcriptome of Primary Human Monocytes: Modulation of Novel Immune-Related Genes and Identification Of CC-Chemokine Ligand 20 as a New Hypoxia-Inducible Gene." The Journal of Immunology 177(3): 1941-1955.
- Campbell, Eric L., Walter J. Bruyninckx, Caleb J. Kelly, Louise E. Glover, Eóin N. McNamee, Brittelle E. Bowers, Amanda J. Bayless, M. Scully, Bejan J. Saeedi, L. Golden-Mason, Stefan F. Ehrentraut, Valerie F. Curtis, A. Burgess, John F. Garvey, A. Sorensen, R. Nemenoff, P. Jedlicka, Cormac T. Taylor, Douglas J. Kominsky and Sean P. Colgan (2014). "Transmigrating Neutrophils Shape the Mucosal Microenvironment through Localized Oxygen Depletion to Influence Resolution of Inflammation." Immunity 40(1): 66-77.
- Cardani, A., A. Boulton, T. S. Kim and T. J. Braciale (2017). "Alveolar Macrophages Prevent Lethal Influenza Pneumonia By Inhibiting Infection Of Type-1 Alveolar Epithelial Cells." PLOS Pathogens 13(1): e1006140.
- Carreau, A., B. El Hafny-Rahbi, A. Matejuk, C. Grillon and C. Kieda (2011). "Why is the partial oxygen pressure of human tissues a crucial parameter? Small molecules and hypoxia." Journal of cellular and molecular medicine 15(6): 1239-1253.
- Chignard, M. and V. Balloy (2000). "Neutrophil recruitment and increased permeability during acute lung injury induced by lipopolysaccharide." American Journal of Physiology-Lung Cellular and Molecular Physiology 279(6): L1083-L1090.
- Cramer, T., Y. Yamanishi, B. E. Clausen, I. Förster, R. Pawlinski, N. Mackman, V. H. Haase, R. Jaenisch, M. Corr, V. Nizet, G. S. Firestein, H. P. Gerber, N. Ferrara and R. S. Johnson (2003). "HIF-1alpha is essential for myeloid cell-mediated inflammation." Cell 112(5): 645-657.
- Delprat, V., C. Tellier, C. Demazy, M. Raes, O. Feron and C. Michiels (2020). "Cycling hypoxia promotes a pro-inflammatory phenotype in macrophages via JNK/p65 signaling pathway." Scientific reports 10(1): 882-882.
- Fan, E. K. Y. and J. Fan (2018). "Regulation of alveolar macrophage death in acute lung inflammation." Respiratory research 19(1): 50-50.
- Freemerman, A. J., A. R. Johnson, G. N. Sacks, J. J. Milner, E. L. Kirk, M. A. Troester, A. N. Macintyre, P. Goraksha-Hicks, J. C. Rathmell and L. Makowski (2014). "Metabolic reprogramming of macrophages: glucose transporter 1 (GLUT1)-mediated glucose metabolism drives a proinflammatory phenotype." The Journal of biological chemistry 289(11): 7884-7896.

Fröhlich, S., J. Boylan and P. McLoughlin (2013). "Hypoxia-Induced Inflammation in the Lung." American Journal of Respiratory Cell and Molecular Biology 48(3): 271-279.

Ghoneim, H. E., P. G. Thomas and J. A. McCullers (2013). "Depletion of Alveolar Macrophages during Influenza Infection Facilitates Bacterial Superinfections." The Journal of Immunology 191(3): 1250.

Gibbins, S. L., R. Goyal, A. N. Desch, S. M. Leach, M. Prabagar, S. M. Atif, D. L. Bratton, W. Janssen and C. V. Jakubzick (2015). "Transcriptome analysis highlights the conserved difference between embryonic and postnatal-derived alveolar macrophages." Blood 126(11): 1357-1366.

Grant, R. A., L. Morales-Nebreda, N. S. Markov, S. Swaminathan, M. Querrey, E. R. Guzman, D. A. Abbott, H. K. Donnelly, A. Donayre, I. A. Goldberg, Z. M. Klug, N. Borkowski, Z. Lu, H. Kihshen, Y. Politanska, L. Sichizya, M. Kang, A. Shilatifard, C. Qi, J. W. Lomasney, A. C. Argento, J. M. Kruser, E. S. Malsin, C. O. Pickens, S. B. Smith, J. M. Walter, A. E. Pawlowski, D. Schneider, P. Nannapaneni, H. Abdala-Valencia, A. Bharat, C. J. Gottardi, G. R. S. Budinger, A. V. Misharin, B. D. Singer, R. G. Wunderink, R. A. Grant, L. Morales-Nebreda, N. S. Markov, S. Swaminathan, M. Querrey, E. R. Guzman, D. A. Abbott, H. K. Donnelly, A. Donayre, I. A. Goldberg, Z. M. Klug, N. Borkowski, Z. Lu, H. Kihshen, Y. Politanska, L. Sichizya, M. Kang, A. Shilatifard, C. Qi, J. W. Lomasney, A. C. Argento, J. M. Kruser, E. S. Malsin, C. O. Pickens, S. B. Smith, J. M. Walter, A. E. Pawlowski, D. Schneider, P. Nannapaneni, H. Abdala-Valencia, A. Bharat, C. J. Gottardi, G. R. S. Budinger, A. V. Misharin, B. D. Singer, R. G. Wunderink, A. A. Wagh, A. R. Hauser, A. R. Wolfe, A. Thakrar, A. V. Yeldandi, A. A. Wang, A. R. Levenson, A. M. Joudi, B. Tran, C. A. Gao, C. Kurihara, C. J. Schroedl, C. M. Horvath, D. Meza, D. D. Odell, D. W. Kamp, D. R. Winter, E. A. Ozer, E. D. Shanes, E. T. Bartom, E. J. Rendleman, E. M. Leibenguth, F. Wehbe, G. Y. Liu, G. T. Gadhvi, H. T. Navarro, J. I. Sznajder, J. E. Dematte, J. Le, J. M. Arnold, J. C. Du, J. Coleman, J. I. Bailey, J. S. Deters, J. A. Fiala, J. Starren, K. M. Ridge, K. Secunda, K. Aren, K. L. Gates, K. Todd, L. D. Gradone, L. N. Textor, L. F. Wolfe, L. L. Pesce, L. A. Nunes Amaral, M. L. Rosenbaum, M. Kandpal, M. Jain, M. A. Sala, M. Saine, M. Carns, M. J. Alexander, M. J. Cuttica, M. H. Prickett, N. H. Khan, N. S. Chandel, N. D. Soulaakis, O. R. Rivas, P. C. Seed, P. A. Reyfman, P. D. Go, P. H. S. Sporn, P. R. Cooper, R. Tomic, R. Patel, R. Garza-Castillon, R. Kalhan, R. I. Morimoto, R. J. Mylvaganam, S. S. Kim, S. W. M. Gatesy, S. Thakkar, S. Ben Maamar, S. Han, S. R. Rosenberg, S. Nozick, S. J. Green, S. R. Russell, T. A. Poor, T. J. Zak, T. A. Lombardo, T. Stoeger, T. Shamaly, Z. Ren and N. U. S. S. I. The (2021). "Circuits between infected macrophages and T cells in SARS-CoV-2 pneumonia." Nature 590(7847): 635-641.

Gross, M. W., U. Karbach, K. Groebe, A. J. Franko and W. Mueller-Klieser (1995). "Calibration of misonidazole labeling by simultaneous measurement of oxygen tension and labeling density in multicellular spheroids." Int J Cancer 61(4): 567-573.

Guilliams, M., I. De Kleer, S. Henri, S. Post, L. Vanhoutte, S. De Prijck, K. Deswarte, B. Malissen, H. Hammad and B. N. Lambrecht (2013). "Alveolar macrophages develop from fetal monocytes that differentiate into long-lived cells in the first week of life via GM-CSF." Journal of Experimental Medicine 210(10): 1977-1992.

Hofer, C. C., P. S. Woods and I. C. Davis (2015). "Infection of mice with influenza A/WSN/33 (H1N1) virus alters alveolar type II cell phenotype." American Journal of Physiology-Lung Cellular and Molecular Physiology 308(7): L628-L638.

Holt, P. G., J. Oliver, N. Bilyk, C. McMenamin, P. G. McMenamin, G. Kraal and T. Thepen (1993). "Downregulation of the antigen presenting cell function(s) of pulmonary dendritic cells in vivo by resident alveolar macrophages." Journal of Experimental Medicine 177(2): 397-407.

Hussell, T. and T. J. Bell (2014). "Alveolar macrophages: plasticity in a tissue-specific context." Nature Reviews Immunology 14(2): 81-93.

Ip, W. K. E., N. Hoshi, D. S. Shouval, S. Snapper and R. Medzhitov (2017). "Anti-inflammatory effect of IL-10 mediated by metabolic reprogramming of macrophages." Science (New York, N.Y.) 356(6337): 513-519.

Izquierdo, H. M., P. Brandi, M.-J. Gómez, R. Conde-Garrosa, E. Priego, M. Enamorado, S. Martínez-Cano, I. Sánchez, L. Conejero, D. Jimenez-Carretero, S. Martín-Puig, M. Williams and D. Sancho (2018). "Von Hippel-Lindau Protein Is Required for Optimal Alveolar Macrophage Terminal Differentiation, Self-Renewal, and Function." Cell reports 24(7): 1738-1746.

Jakubzick, C., F. Tacke, J. Llodra, N. van Rooijen and G. J. Randolph (2006). "Modulation of Dendritic Cell Trafficking to and from the Airways." The Journal of Immunology 176(6): 3578-3584.

Jaworska, J., F. Coulombe, J. Downey, F. Tzelepis, K. Shalaby, I. Tattoli, J. Berube, S. Rousseau, J. G. Martin, S. E. Girardin, J. A. McCullers and M. Divangahi (2014). "NLRX1 prevents mitochondrial induced apoptosis and enhances macrophage antiviral immunity by interacting with influenza virus PB1-F2 protein." Proc Natl Acad Sci U S A 111(20): E2110-2119.

Kam Y, S. P., Dranka BP (2017). "Real time discrimination of inflammatory macrophage activation using Agilent Seahorse XF technology (white paper)."

Kim, H. M., Y. W. Lee, K. J. Lee, H. S. Kim, S. W. Cho, N. van Rooijen, Y. Guan and S. H. Seo (2008). "Alveolar macrophages are indispensable for controlling influenza viruses in lungs of pigs." J Virol 82(9): 4265-4274.

Knapp, S., J. C. Leemans, S. Florquin, J. Branger, N. A. Maris, J. Pater, N. v. Rooijen and T. v. d. Poll (2003). "Alveolar Macrophages Have a Protective Antiinflammatory Role during Murine Pneumococcal Pneumonia." American Journal of Respiratory and Critical Care Medicine 167(2): 171-179.

Kong, D., E. J. Park, A. G. Stephen, M. Calvani, J. H. Cardellina, A. Monks, R. J. Fisher, R. H. Shoemaker and G. Melillo (2005). "Echinomycin, a Small-Molecule Inhibitor of Hypoxia-Inducible Factor-1 DNA-Binding Activity." Cancer Research 65(19): 9047-9055.

Lavin, Y., D. Winter, R. Blecher-Gonen, E. David, H. Keren-Shaul, M. Merad, S. Jung and I. Amit (2014). "Tissue-resident macrophage enhancer landscapes are shaped by the local microenvironment." Cell 159(6): 1312-1326.

Leach, S. M., S. L. Gibbings, A. D. Tewari, S. M. Atif, B. Vestal, T. Danhorn, W. J. Janssen, T. D. Wager and C. V. Jakubzick (2020). "Human and Mouse Transcriptome Profiling Identifies Cross-Species Homology in Pulmonary and Lymph Node Mononuclear Phagocytes." Cell Rep 33(5): 108337.

Liao, M., Y. Liu, J. Yuan, Y. Wen, G. Xu, J. Zhao, L. Cheng, J. Li, X. Wang, F. Wang, L. Liu, I. Amit, S. Zhang and Z. Zhang (2020). "Single-cell landscape of bronchoalveolar immune cells in patients with COVID-19." Nature Medicine 26(6): 842-844.

Machado-Aranda, D., M. V Suresh, B. Yu, V. Dolgachev, M. R. Hemmila and K. Raghavendran (2014). "Alveolar macrophage depletion increases the severity of acute inflammation following nonlethal unilateral lung contusion in mice." The journal of trauma and acute care surgery 76(4): 982-990.

Matak, P., M. Heinis, J. R. R. Mathieu, R. Corriden, S. Cuvellier, S. Delga, R. Mounier, A. Rouquette, J. Raymond, D. Lamarque, J.-F. Emile, V. Nizet, E. Touati and C. Peyssonnaux (2015). "Myeloid HIF-1 Is Protective in Helicobacter pylori-Mediated Gastritis." The Journal of Immunology 194(7): 3259.

Maus, U., K. v. Grote, W. A. Kuziel, M. Mack, E. J. Miller, J. Cihak, M. Stangassinger, R. Maus, D. Schlöndorff, W. Seeger and J. Lohmeyer (2002). "The Role of CC Chemokine Receptor 2 in Alveolar Monocyte and Neutrophil Immigration in Intact Mice." American Journal of Respiratory and Critical Care Medicine 166(3): 268-273.

Maus, U., S. Herold, H. Muth, R. Maus, L. Ermert, M. Ermert, N. Weissmann, S. Rosseau, W. Seeger, F. Grimminger and J. Lohmeyer (2001). "Monocytes recruited into the alveolar air

space of mice show a monocytic phenotype but upregulate CD14." American Journal of Physiology-Lung Cellular and Molecular Physiology 280(1): L58-L68.

McQuattie-Pimentel, A. C., Z. Ren, N. Joshi, S. Watanabe, T. Stoeger, M. Chi, Z. Lu, L. Sichizya, R. P. Aillon, C.-I. Chen, S. Soberanes, Z. Chen, P. A. Reyfman, J. M. Walter, K. R. Anekalla, J. M. Davis, K. A. Helmin, C. E. Runyan, H. Abdala-Valencia, K. Nam, A. Y. Meliton, D. R. Winter, R. I. Morimoto, G. M. Mutlu, A. Bharat, H. Perlman, C. J. Gottardi, K. M. Ridge, N. S. Chandel, J. I. Sznajder, W. E. Balch, B. D. Singer, A. V. Misharin and G. R. S. Budinger (2021). "The lung microenvironment shapes a dysfunctional response of alveolar macrophages in aging." The Journal of clinical investigation 131(4): e140299.

Misharin, A. V., L. Morales-Nebreda, G. M. Mutlu, G. R. S. Budinger and H. Perlman (2013). "Flow cytometric analysis of macrophages and dendritic cell subsets in the mouse lung." American journal of respiratory cell and molecular biology 49(4): 503-510.

Nelson, B., X. Zhou, M. White, K. Hartshorn, K. Takahashi, T. B. Kinane, A. Anandaiah and H. Koziel (2014). "Recombinant human mannose-binding lectin dampens human alveolar macrophage inflammatory responses to influenza A virus in vitro." J Leukoc Biol 95(5): 715-722.

Palsson-McDermott, E. M., A. M. Curtis, G. Goel, M. A. Lauterbach, F. J. Sheedy, L. E. Gleeson, M. W. van den Bosch, S. R. Quinn, R. Domingo-Fernandez, D. G. Johnston, J. K. Jiang, W. J. Israelsen, J. Keane, C. Thomas, C. Clish, M. Vander Heiden, R. J. Xavier and L. A. O'Neill (2015). "Pyruvate kinase M2 regulates Hif-1 α activity and IL-1 β induction and is a critical determinant of the warburg effect in LPS-activated macrophages." Cell Metab 21(1): 65-80.

Peyssonnaud, C., V. Datta, T. Cramer, A. Doedens, E. A. Theodorakis, R. L. Gallo, N. Hurtado-Ziola, V. Nizet and R. S. Johnson (2005). "HIF-1 α expression regulates the bactericidal capacity of phagocytes." The Journal of clinical investigation 115(7): 1806-1815.

Roiniotis, J., H. Dinh, P. Masendycz, A. Turner, C. L. Elsegood, G. M. Scholz and J. A. Hamilton (2009). "Hypoxia Prolongs Monocyte/Macrophage Survival and Enhanced Glycolysis Is Associated with Their Maturation under Aerobic Conditions." The Journal of Immunology 182(12): 7974-7981.

Schaible, B., K. Schaffer and C. T. Taylor (2010). "Hypoxia, innate immunity and infection in the lung." Respir Physiol Neurobiol 174(3): 235-243.

Schneider, C., S. P. Nobs, A. K. Heer, M. Kurrer, G. Klinke, N. van Rooijen, J. Vogel and M. Kopf (2014). "Alveolar Macrophages Are Essential for Protection from Respiratory Failure and Associated Morbidity following Influenza Virus Infection." PLOS Pathogens 10(4): e1004053.

Schousboe, P., A. Ronit, H. B. Nielsen, T. Benfield, L. Wiese, N. Scoutaris, H. Verder, R. M. G. Berg, P. Verder and R. R. Plovsing (2022). "Reduced levels of pulmonary surfactant in COVID-19 ARDS." Sci Rep 12(1): 4040.

Semenza, G. L. (2012). "Hypoxia-inducible factors in physiology and medicine." Cell 148(3): 399-408.

Shannon, P., A. Markiel, O. Ozier, N. S. Baliga, J. T. Wang, D. Ramage, N. Amin, B. Schwikowski and T. Ideker (2003). "Cytoscape: a software environment for integrated models of biomolecular interaction networks." Genome research 13(11): 2498-2504.

Short, K. R., E. J. B. V. Kroeze, R. A. M. Fouchier and T. Kuiken (2014). "Pathogenesis of influenza-induced acute respiratory distress syndrome." The Lancet Infectious Diseases 14(1): 57-69.

Singh, A., J. W. Wilson, C. J. Schofield and R. Chen (2020). "Hypoxia-inducible factor (HIF) prolyl hydroxylase inhibitors induce autophagy and have a protective effect in an in-vitro ischaemia model." Scientific Reports 10(1): 1597.

Spencer, J. A., F. Ferraro, E. Roussakis, A. Klein, J. Wu, J. M. Runnels, W. Zaher, L. J. Mortensen, C. Alt, R. Turcotte, R. Yusuf, D. Côté, S. A. Vinogradov, D. T. Scadden and C. P. Lin (2014). "Direct measurement of local oxygen concentration in the bone marrow of live animals." Nature 508(7495): 269-273.

918 Svedberg, F. R., S. L. Brown, M. Z. Krauss, L. Campbell, C. Sharpe, M. Clausen, G. J. Howell,
 919 H. Clark, J. Madsen, C. M. Evans, T. E. Sutherland, A. C. Ivens, D. J. Thornton, R. K. Grencis,
 920 T. Hussell, D. M. Cunoosamy, P. C. Cook and A. S. MacDonald (2019). "The lung environment
 921 controls alveolar macrophage metabolism and responsiveness in type 2 inflammation." Nature
 922 Immunology 20(5): 571-580.
 923 Tannahill, G. M., A. M. Curtis, J. Adamik, E. M. Palsson-McDermott, A. F. McGettrick, G. Goel,
 924 C. Frezza, N. J. Bernard, B. Kelly, N. H. Foley, L. Zheng, A. Gardet, Z. Tong, S. S. Jany, S. C.
 925 Corr, M. Haneklaus, B. E. Caffrey, K. Pierce, S. Walmsley, F. C. Beasley, E. Cummins, V. Nizet,
 926 M. Whyte, C. T. Taylor, H. Lin, S. L. Masters, E. Gottlieb, V. P. Kelly, C. Clish, P. E. Auron, R. J.
 927 Xavier and L. A. J. O'Neill (2013). "Succinate is an inflammatory signal that induces IL-1 β
 928 through HIF-1 α ." Nature 496(7444): 238-242.
 929 Thepen, T., N. Van Rooijen and G. Kraal (1989). "Alveolar macrophage elimination in vivo is
 930 associated with an increase in pulmonary immune response in mice." Journal of Experimental
 931 Medicine 170(2): 499-509.
 932 Traylor, Z. P., F. Aeffner and I. C. Davis (2013). "Influenza A H1N1 induces declines in alveolar
 933 gas exchange in mice consistent with rapid post-infection progression from acute lung injury to
 934 ARDS." Influenza Other Respir Viruses 7(3): 472-479.
 935 Vichai, V. and K. Kirtikara (2006). "Sulforhodamine B colorimetric assay for cytotoxicity
 936 screening." Nature Protocols 1(3): 1112-1116.
 937 Ware, L. B. and M. A. Matthay (2000). "The Acute Respiratory Distress Syndrome." New
 938 England Journal of Medicine 342(18): 1334-1349.
 939 Whitsett, J. A., S. E. Wert and T. E. Weaver (2010). "Alveolar surfactant homeostasis and the
 940 pathogenesis of pulmonary disease." Annu Rev Med 61: 105-119.
 941 Wolk, K. E., E. R. Lazarowski, Z. P. Traylor, E. N. Yu, N. A. Jewell, R. K. Durbin, J. E. Durbin
 942 and I. C. Davis (2008). "Influenza A virus inhibits alveolar fluid clearance in BALB/c mice." Am J
 943 Respir Crit Care Med 178(9): 969-976.
 944 Woods, P. S., L. M. Doolittle, L. E. Rosas, L. M. Joseph, E. P. Calomeni and I. C. Davis (2016).
 945 "Lethal H1N1 influenza A virus infection alters the murine alveolar type II cell surfactant
 946 lipidome." American Journal of Physiology-Lung Cellular and Molecular Physiology 311(6):
 947 L1160-L1169.
 948 Woods, P. S., L. M. Kimmig, A. Y. Meliton, K. A. Sun, Y. Tian, E. M. O'Leary, G. A. Gökalp, R.
 949 B. Hamanaka and G. M. Mutlu (2020). "Tissue-Resident Alveolar Macrophages Do Not Rely on
 950 Glycolysis for LPS-induced Inflammation." Am J Respir Cell Mol Biol 62(2): 243-255.
 951 Worlitzsch, D., R. Tarran, M. Ulrich, U. Schwab, A. Cekici, K. C. Meyer, P. Birrer, G. Bellon, J.
 952 Berger, T. Weiss, K. Botzenhart, J. R. Yankaskas, S. Randell, R. C. Boucher and G. Döring
 953 (2002). "Effects of reduced mucus oxygen concentration in airway Pseudomonas infections of
 954 cystic fibrosis patients." J Clin Invest 109(3): 317-325.
 955 Wu, G., X. Feng and L. Stein (2010). "A human functional protein interaction network and its
 956 application to cancer data analysis." Genome Biology 11(5): R53.
 957 Xi, Y., T. Kim, A. N. Brumwell, I. H. Driver, Y. Wei, V. Tan, J. R. Jackson, J. Xu, D. K. Lee, J. E.
 958 Gotts, M. A. Matthay, J. M. Shannon, H. A. Chapman and A. E. Vaughan (2017). "Local lung
 959 hypoxia determines epithelial fate decisions during alveolar regeneration." Nat Cell Biol 19(8):
 960 904-914.
 961 Xie, M., Y. Yu, R. Kang, S. Zhu, L. Yang, L. Zeng, X. Sun, M. Yang, T. R. Billiar, H. Wang, L.
 962 Cao, J. Jiang and D. Tang (2016). "PKM2-dependent glycolysis promotes NLRP3 and AIM2
 963 inflammasome activation." Nature communications 7: 13280-13280.
 964 Zhu, B., Y. Wu, S. Huang, R. Zhang, Y. M. Son, C. Li, I. S. Cheon, X. Gao, M. Wang, Y. Chen,
 965 X. Zhou, Q. Nguyen, A. T. Phan, S. Behl, M. M. Taketo, M. Mack, V. S. Shapiro, H. Zeng, H.
 966 Ebihara, J. J. Mullon, E. S. Edell, J. S. Reisenauer, N. Demirel, R. M. Kern, R. Chakraborty, W.
 967 Cui, M. H. Kaplan, X. Zhou, A. W. Goldrath and J. Sun (2021). "Uncoupling of macrophage

968 inflammation from self-renewal modulates host recovery from respiratory viral infection."
969 Immunity 54(6): 1200-1218.e1209.
970

FIGURE LEGENDS

Figure 1. Tissue-resident alveolar macrophages exhibit HIF-1 α stabilization and develop a glycolytic phenotype in response to hypoxia, while BMDMs have limited metabolic adaptation to hypoxia. TR-AMs (**A-E**) and BMDMs (**F-J**) were incubated overnight (16h) at varying O₂ concentrations. **(A)** Using Seahorse XF24 analyzer, glycolysis was measured as extracellular acidification rate (ECAR). TR-AMs were sequentially treated with glucose, oligomycin (ATP synthase inhibitor) and 2-deoxyglucose (2-DG) (inhibitor of hexokinase 2, or glycolysis). **(B)** Interleaved scatter plots quantifying glycolytic parameters. Data represent at least 3 independent experiments (n=4 separate wells per group). Glycolytic parameters were compared against 21% O₂ and significance was determined by one-way ANOVA with Bonferroni correction. **(C)** Western blot analysis of nuclear extract to assess HIF-1 α expression in TR-AMs treated with different concentrations of O₂. DMOG served as a positive control **(D)** Glycolysis stress test of TR-AMs under 1.5% O₂ in combination with echinomycin (16h). **(E)** Western blot analysis of whole cell lysates of TR-AMs treated with 21% or 1.5% O₂ in combination with echinomycin (16h). **(F)** BMDM glycolysis measurements (ECAR) using Seahorse XF24 analyzer. **(G)** Interleaved scatter plots quantifying glycolytic parameters. Data represent at least 3 independent experiments (n=4 separate wells per group). Glycolytic parameters were compared against 21% O₂ and significance was determined by one-way ANOVA with Bonferroni correction. **(H)** Western blot analysis of nuclear extract to assess HIF-1 α expression in BMDMs treated with different concentrations of O₂. **(I)** Glycolysis stress test of BMDMs under 1.5% O₂ in combination with echinomycin (16h). **(J)** Western blot analysis of whole cell lysates of BMDMs treated with 21% or 1.5% O₂ in combination with echinomycin (16h). All error bars denote mean \pm SD. *p < 0.05.

Figure 1-figure supplement 1. Knockdown of *Hif1a* diminishes hypoxia-induced glycolytic phenotype in TR-AMs. TR-AMs (**A-C**) and BMDMs (**D-F**) were transfected with *Hif1a* or control siRNA and subsequently incubated overnight (16h) at 21% or 1.5% O₂. Western blot analysis of nuclear extracts to assess successful *Hif1a* knockdown in (**A**) TR-AMs and (**D**) BMDMs under 1.5% O₂. Western blot analysis of whole cell extracts from (**B**) TR-AMs and (**E**) BMDMs. Extracellular lactate levels in (**C**) TR-AMs and (**F**) BMDMs incubated overnight (16h) at 21% or 1.5% O₂. Significance was determined by two-way ANOVA with Bonferroni correction. All error bars denote mean \pm SD. *p < 0.05.

Figure 1-figure supplement 2. Prolonged but not short-term hypoxia induces glycolysis in TR-AMs. TR-AMs (**A-C**) or BMDMs (**D-F**) were incubated for 2h or overnight (16h) at 1.5% O₂. (**A**) Western blot analysis of TR-AM (**A**) and BMDM (**D**) nuclear extracts to assess HIF-1 α protein expression. Using Seahorse XF24 technology, TR-AM (**B**) and BMDM (**E**) glycolysis was measured as extracellular acidification rate (ECAR). Interleaved scatter plots quantifying glycolytic parameters in TR-AMs (**C**) and BMDMs (**F**). Data represents at least 3 independent experiments (n=4 separate wells per group). Significance was determined by unpaired, two-tailed t-test. *p < 0.05.

Figure 2. The hypoxia-induced transcriptomic response differs substantially between TR-AMs and BMDMs. TR-AMs and BMDMs were incubated overnight (16h) under normoxia (21.0% O₂) or hypoxia (1.5% O₂). (**A**) Venn diagrams show differentially expressed genes (DEGs) altered by hypoxia in TR-AMs (741 total DEGs), and BMDMs (260 total DEGs). DEGs were identified using DESeq2 at FC>2 and FDR adjusted p-value of p<0.05. (**B**) Reactome pathway enrichment comparing number of genes in a given pathway altered by hypoxia in TR-AMs and BMDMs. (**C**) Heatmap representing the top 20 significant metabolic genes altered by hypoxia in both TR-AMs and BMDMs. (**D**) Western blot analysis of nuclear extracts to assess

HIF-1 α protein expression. **(E)** Western blot analysis of whole cell extracts to assess glycolytic enzyme (HK2, LDH) and prolyl hydroxylase (PHD2, PHD3) protein expression

Figure 3. Hypoxia modulates TR-AM cytokine production and metabolic response to LPS.

TR-AMs were incubated overnight (16h) under 21% or 1.5% O₂ then stimulated with 20ng/ml LPS for 6 while maintaining pretreatment conditions. For IL-1 β measurements, 5mM ATP was added to TR-AMs for 30 minutes following 6h LPS treatment to activate caspase 1, ensuring IL-1 β release. **(A)** We measured cytokine (TNF α , IL-6, KC, CCL2 and IL-1 β) levels in media using ELISA. Data represent at least 3 independent experiments; n=3 per group. Significance was determined by unpaired, two-tailed t-test **(B)** qPCR was used to measure mRNA expression (*Tnfa*, *Il6*, *Kc*, *Ccl2*, and *Il1b*). Gene expression was normalized to corresponding gene ct values in 21% group and represented as fold change using the $\Delta\Delta$ ct method. Data represent at least 3 independent experiments; n=3 per group. Significance was determined by unpaired, two-tailed t-test **(C)** Western blot analysis of whole cell extracts at 6 and 24h post LPS treatment **(D)** ECAR was measured in following acute LPS injection (final concentration: 20 ng/ml) in TR-AMs conditioned in 1.5% O₂ **(E)** CE-MS metabolite heatmap for glycolytic intermediates. All error bars denote mean \pm SD. *p < 0.05.

Figure 3-figure supplement 1. Hypoxia alters cytokine production in BMDMs. BMDMs were incubated overnight (16h) under normoxia or 1.5% O₂ then stimulated with LPS (20 ng/ml) for 6 hours while maintaining pretreatment conditions. For IL-1 β , 5mM ATP was added to BMDMs for 30 minutes following 6 hours of LPS treatment to activate caspase 1, ensuring IL-1 β release. **(A)** Sandwich ELISA was used to measure secreted cytokine (TNF α , IL-6, KC, CCL2 and IL-1 β). Data represents at least 3 independent experiments; n=3 per group. Significance was determined by unpaired, two-tailed t-test. All error bars denote mean \pm SD. *p < 0.05.

Figure 3-figure supplement 2. LPS induces an immediate increase in glycolysis in BMDMs. ECAR was measured in normoxic BMDMs following acute LPS injection (final concentration: 20 ng/ml).

Figure 4. Hypoxia rescues ETC inhibitor-induced cell death and impaired cytokine production in TR-AMs. (A) Mitochondrial stress test to measure oxygen consumption rate (OCR) using Seahorse XF24 in TR-AMs, which were treated sequentially with oligomycin (ATP synthase inhibitor), FCCP (uncoupler) and Rotenone (Rot)/Antimycin A (Ant) (complex I and III inhibitors, respectively). **(B)** Interleaved scatter plots quantifying mitochondrial respiration parameters. Data represents at least 3 experiments (n=4 separate wells per group). Mitochondrial parameters were compared against 21% O₂ and significance was determined by one-way ANOVA with Bonferroni correction **(C)** ECAR measurement during mitochondrial stress test to visualize TR-AMs ability to upregulate glycolysis in response to mitochondrial inhibition **(D)** TR-AMs were incubated overnight (16h) under 21% or 1.5% O₂ then stimulated with 20ng/ml LPS in the presence of absence of mitochondrial inhibitors (20nM Ant or Rot) for 6 hours while maintaining pretreatment conditions. ELISA was used to measure secreted cytokine (TNF α , IL-6, KC, CCL2, and IL-1 β) levels in media. ATP added to cells prior to collection for IL-1 β assessment. Data represent at least 3 independent experiments; n=3 per group. Significance was determined by one-way ANOVA with Bonferroni correction. **(E)** TR-AMs were cultured under 21% or 1.5% O₂ for 6h then treated with mitochondrial inhibitors (100nM Ant or 500nM Rot) overnight and an Sulforhodamine B assay was performed to measure cytotoxicity. Graphs represent cell viability compared to control, 21% O₂ group. Data represent at least 3 independent experiments (n=3 per group). Significance was determined by two-way ANOVA with Bonferroni correction. All error bars denote mean \pm SD. *p < 0.05.

Figure 4-figure supplement 1. The effect of hypoxia on BMDM mitochondrial function, cytokine production and cell liability under ETC inhibition. (A) Mitochondrial stress test to measure oxygen consumption rate (OCR) using Seahorse XF24 in BMDMs. **(B)** Interleaved scatter plots quantifying mitochondrial respiration parameters. Data represents at least 3 experiments (n=4 separate wells per group). Mitochondrial parameters were compared against 21% O₂ and significance was determined by one-way ANOVA with Bonferroni correction **(C)** ECAR measurement during mitochondrial stress test. **(D)** BMDMs were incubated overnight (16h) under 21% or 1.5% O₂ then stimulated with 20ng/ml LPS in the presence or absence of mitochondrial inhibitors (20nM Antimycin A (Ant) or Rotenone (Rot)) for 6 hours while maintaining pretreatment conditions. ELISA was used to measure secreted cytokine (TNF α , IL-6, KC, CCL2, and IL-1 β) levels in media. ATP added to cells prior to collection for IL-1 β assessment. Data represent at least 3 independent experiments; n=3 per group. Significance was determined by one-way ANOVA with Bonferroni correction. **(E)** BMDMs were cultured under 21% or 1.5% O₂ for 6h then treated with mitochondrial inhibitors (100nM Ant or 500nM Rot) overnight and an Sulforhodamine B assay was performed to measure cytotoxicity. Graphs represent cell viability compared to control, 21% O₂ group. Data represent at least 3 independent experiments (n=3 per group). Significance was determined by two-way ANOVA with Bonferroni correction. All error bars denote mean \pm SD. *p < 0.05.

Figure 5. TR-AM survival correlates with a shift to glycolytic metabolism during influenza-induced acute lung injury (A) FACS plots of BALF samples collected from C57BL/6 mice infected with PR8 (100 PFU) at baseline (D0), 3 days (D3) and 6 days (D6) post infection. First, debris, red blood cells, and lymphocytes were eliminated based on size (FSC) and granularity (SSC). Samples were first gated on single cells based on the side scatter (SSC)/forward scatter signal (FSC), and then live cells were selected (SYTOX Green⁻). Ly6G⁻ used to exclude neutrophils. TR-AMs were identified as being PKH26⁺, and

1099 nonresident/infiltrating Mo-AMs were PKH26⁻. Gene expression heatmaps representing (B)
1100 oxidative phosphorylation and (C) glycolytic gene expression. Heatmaps were generated
1101 through DEG analysis of UniProt oxidative phosphorylation and glycolysis gene sets for FAC
1102 TR-AMs (PKH⁺; n=3/group) and Mo-AMs (PKH26⁻ ; n=2/group) over the infection time course.
1103

1104 **Figure 6. Non-hypoxic stabilization of HIF-1 α increases TR-AM survival and improves**
1105 **outcomes in influenza-induced acute lung injury.** TR-AMs were treated (16h) overnight \pm
1106 FG-4592 (25.0 μ M when not stated otherwise). (A) Glycolysis was measured as extracellular
1107 acidification rate (ECAR). (B) Quantification of glycolytic parameters. Data represent at least 3
1108 independent experiments (n=4 separate wells per group). Glycolytic parameters compared to
1109 control group (0.0 μ M) and significance was determined by one-way ANOVA with Bonferroni
1110 correction (C) Western blot analysis of whole cell lysate. (D) nuclear extract. (E) Mitochondrial
1111 stress test to measure oxygen consumption rate (OCR). (F) Quantification of mitochondrial
1112 respiration parameters. Data represents at least 3 experiments (n=4 separate wells per group).
1113 Mitochondrial parameters were compared to control group (0.0 μ M) and significance was
1114 determined by one-way ANOVA with Bonferroni correction (G) ECAR measurement during
1115 mitochondrial stress test. (H) TR-AMs were pretreated overnight (16h) with 0.0 μ M (no
1116 treatment) or 25.0 μ M FG-4592 then stimulated with 20ng/ml LPS in the presence of absence of
1117 mitochondrial inhibitors (20nM Antimycin A (Ant) or Rotenone (Rot)) for 6 hours while
1118 maintaining pretreatment conditions. Sandwich ELISA was used to measure secreted cytokine
1119 (TNF α , IL-6, KC and CCL-2). Data represents at least 3 independent experiments; n=3 per
1120 group. (I) TR-AMs were treated with FG-4592 for 6h then treated with mitochondrial inhibitors
1121 (100nM Ant or 500nM Rot) overnight and an SRB assay was performed to measure cytotoxicity.
1122 Bar graphs represent cytotoxicity compared to control, 0.0uM group. Data represents at least 3
1123 independent experiments (n=3 per group). Significance was determined by two-way ANOVA
1124 with Bonferroni correction. All error bars denote mean \pm SD. *p < 0.05.

Figure 7. Non-hypoxic stabilization of HIF-1 α increases TR-AM survival and improves outcomes in influenza-induced acute lung injury. We intratracheally infected C57BL/6 mice with PR8 (100 pfu) and collected bronchoalveolar lavage fluid (BALF) on day 0 (D0) (uninfected) and day 6 (D6) post-infection. Mice also received either the HIF-1 α stabilizer (FG-4592) or vehicle control on D0. **(A)** Representative FACS plot of BALF macrophages. **(B)** BALF protein concentration **(C)** BALF proinflammatory cytokine levels at D6. BALF data generated from 2 separate experiments (n=7 mice/control group and n=8 mice/FG-4592 group) BALF data significance was determined by unpaired, two-tailed t-test. **(D,E)** C57BL/6 mice infected with PR8 (200 pfu) (10 mice/group). **(D)** Weight loss represented as percentage and normalized to D0. **(E)** Survival curve. All error bars denote mean \pm SD. *p < 0.05.

FIGURE SOURCE DATA

Figure 1-source data 1. The effect of different O₂ concentrations on HIF1 α expression in TR-AMs. Uncropped western blot images of HIF-1 α protein expression in TR-AMs under different concentrations of oxygen.

Figure 1-source data 2. The effect of echinomycin on glycolytic enzyme protein expression in TR-AMs. Uncropped western blot images of HK2, LDHA, and α -tubulin in TR-AMs treated with echinomycin under normoxia or hypoxia.

Figure 1-source data 3. The effect of different O₂ concentrations on HIF1 α expression in BMDMs. Uncropped western blot images of HIF-1 α protein expression in BMDMs under different concentrations of oxygen.

Figure 1-source data 4. The effect of echinomycin on glycolytic enzyme protein expression in BMDMs. Uncropped western blot images of HK2, LDHA, and α -tubulin in BMDMs treated with echinomycin under normoxia or hypoxia.

Figure 1-figure supplement 1-source data 1. Validation of *Hif1a* siRNA knockdown in TR-AMs. Uncropped western blot images of HIF1 α protein expression in TR-AMs treated with either control siRNA or two different *Hif1a* siRNAs.

Figure 1-figure supplement 1-source data 2. The effect of *Hif1a* siRNA knockdown on glycolytic enzyme protein expression in TR-AMs under normoxia and hypoxia. Uncropped western blot images of HK2, LDHA and α -tubulin expression in TR-AMs treated with either control siRNA or two different *Hif1a* siRNAs under normoxia or hypoxia.

Figure 1-figure supplement 1-source data 3. Validation of *Hif1a* siRNA knockdown in BMDMs. Uncropped western blot images of HIF1 α protein expression in BMDMs treated with either control siRNA or two different *Hif1a* siRNAs.

Figure 1-figure supplement 1-source data 4. The effect of *Hif1a* siRNA knockdown on glycolytic enzyme protein expression in BMDMs under normoxia and hypoxia. Uncropped western blot images of HK2, LDHA and α -tubulin expression in BMDMs treated with either control siRNA or two different *Hif1a* siRNAs under normoxia or hypoxia.

Figure 1-figure supplement 2-source data 1. Expression HIF-1 α protein in TR-AMs at different time points following exposure to hypoxia. Uncropped western blot images of HIF1 α protein expression in TR-AMs treated with hypoxia for 0, 2, or 16 hours or with DMOG.

1175 **Figure 1-figure supplement 2-source data 2. Expression HIF-1 α protein in BMDMs at**
1176 **different time points following exposure to hypoxia.** Uncropped western blot images of
1177 HIF1 α protein expression in BMDMs treated with hypoxia for 0, 2, or 16 hours or with DMOG.

1178
1179 **Figure 2-source data 1. Read count data for hypoxia-regulated genes in TR-AMs and**
1180 **BMDMs.**

1181
1182 **Figure 2-source data 2. Differences in HIF-1 α expression between TR-AMs and BMDMs**
1183 **under normoxia and hypoxia.** Uncropped western blot images of HIF1 α expression in TR-AMs
1184 and BMDMs treated with normoxia or hypoxia.

1185
1186 **Figure 2-source data 3. Differences in glycolytic enzyme and prolyl hydroxylase protein**
1187 **expression between TR-AMs and BMDMs under normoxia and hypoxia.** Uncropped
1188 western blot images of HK2, LDHA, PHD2, PHD3 and α -tubulin expression in TR-AMs and
1189 BMDMs treated with normoxia or hypoxia.

1190
1191 **Figure 3-source data 1. Changes in LPS-induced expression of proIL-1 β protein in TR-**
1192 **AMs under normoxia and hypoxia.** Uncropped western blot images of proIL-1 β protein in TR-
1193 AMs treated with LPS for 6 or 24 hours under normoxia or hypoxia.

1194
1195 **Figure 5-source data 1. Read counts data for genes of oxidative phosphorylation in TR-**
1196 **AMs and Mo-AMs.**

1197
1198 **Figure 5-source data 2. Read counts data for genes of glycolysis in TR-AMs and Mo-AMs.**

1199

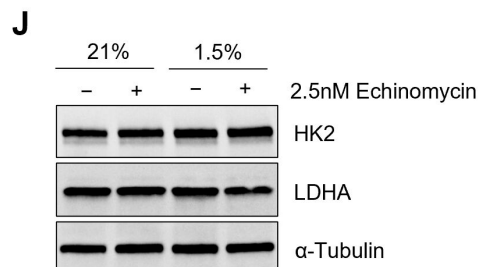
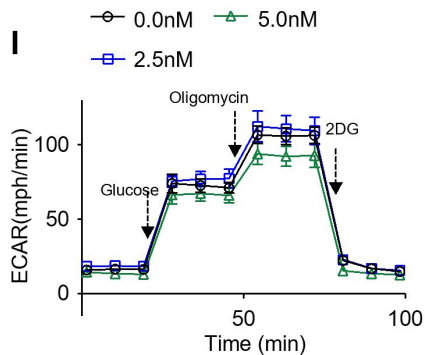
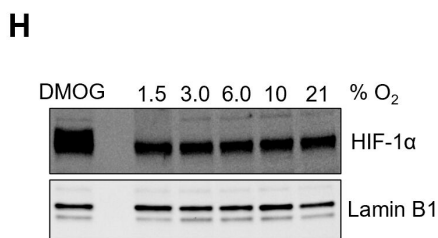
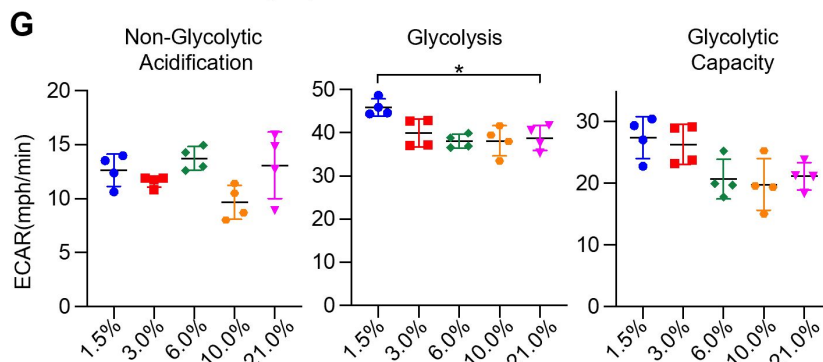
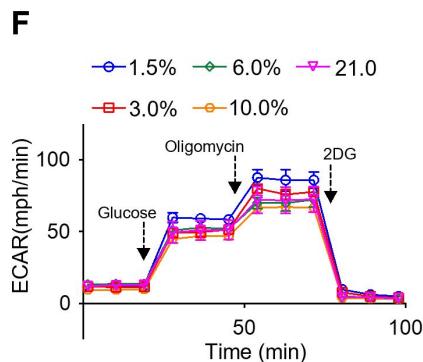
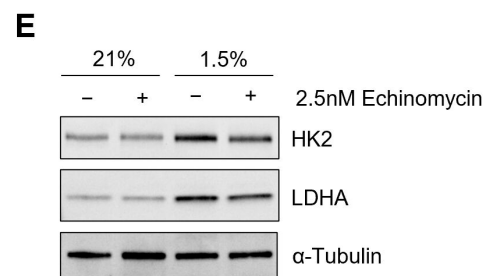
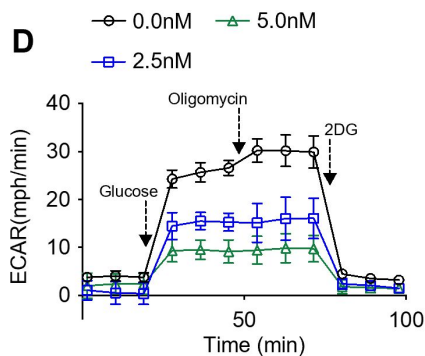
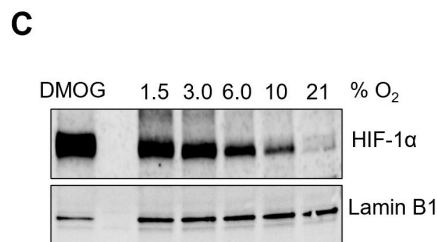
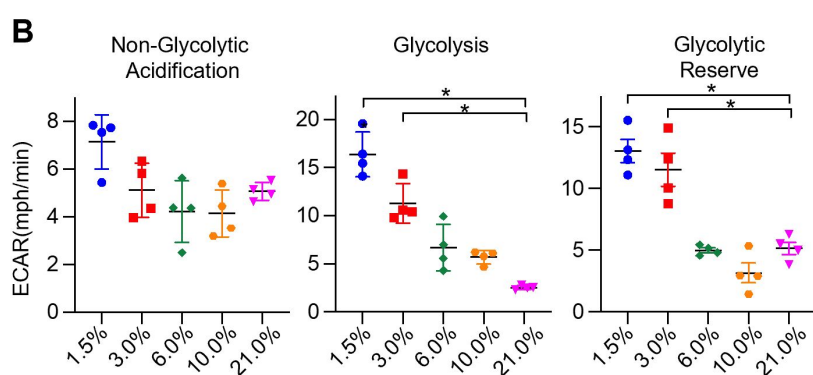
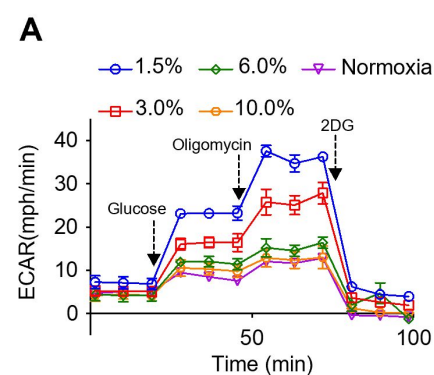
1200 **Figure 6-source data 1. The effect of FG-4592 on HIF-1 α expression in TR-AMs.** Uncropped
1201 western blot images of HIF1 α in TR-AMs treated with FG-4592 or control vehicle.

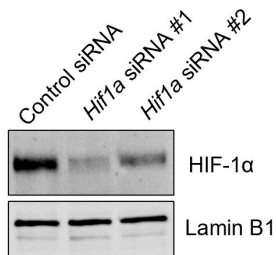
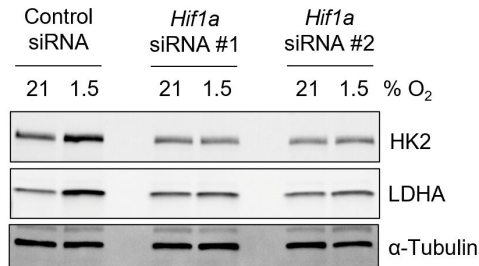
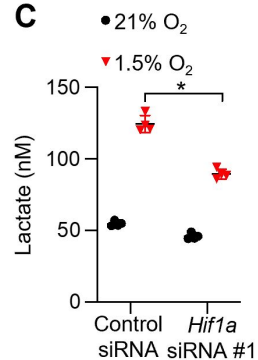
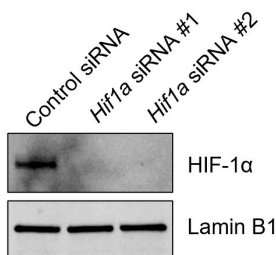
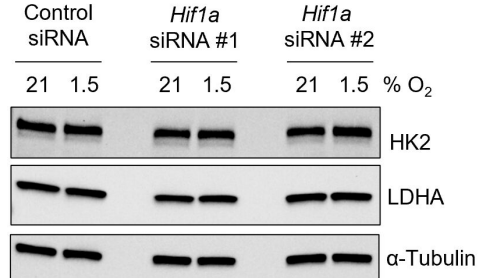
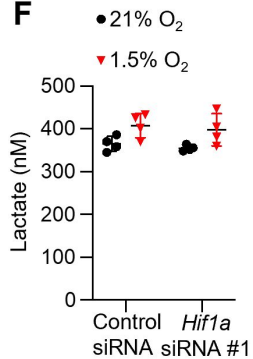
1202

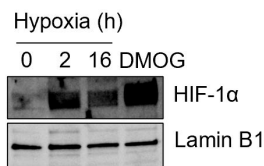
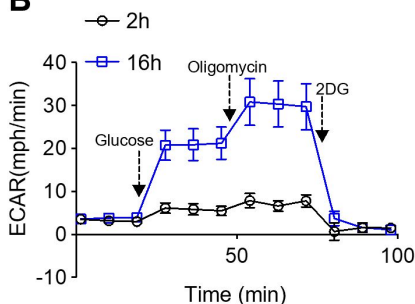
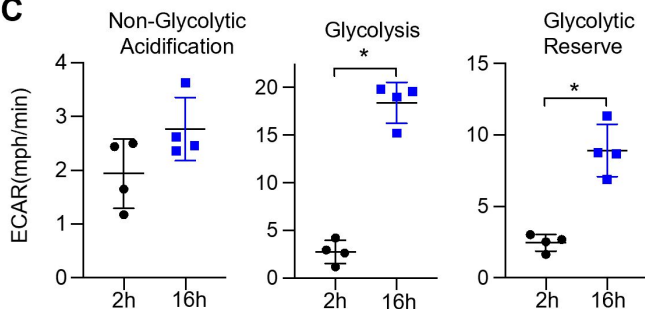
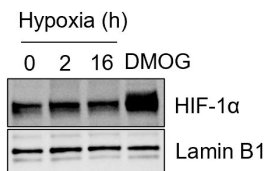
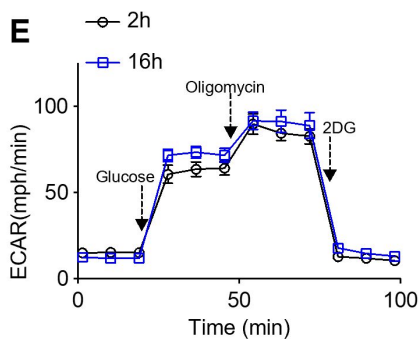
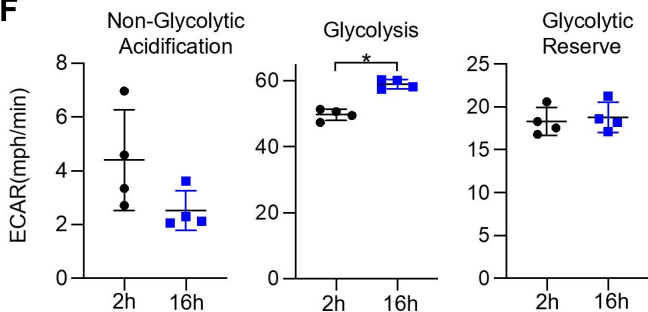
1203 **Figure 6-source data 2. The effect of FG-4592 on glycolytic enzyme and prolyl**
1204 **hydroxylase protein expression in TR-AMs.** Uncropped western blot images of HK2, LDHA,
1205 PHD2, PHD3 and α -tubulin in TR-AMs treated with FG-4592 or control vehicle

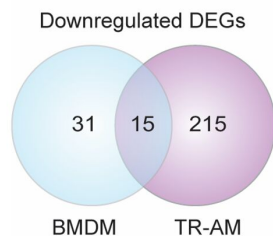
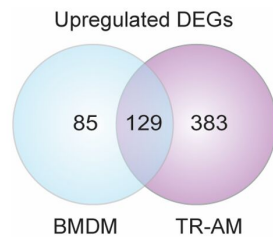
1206

1207

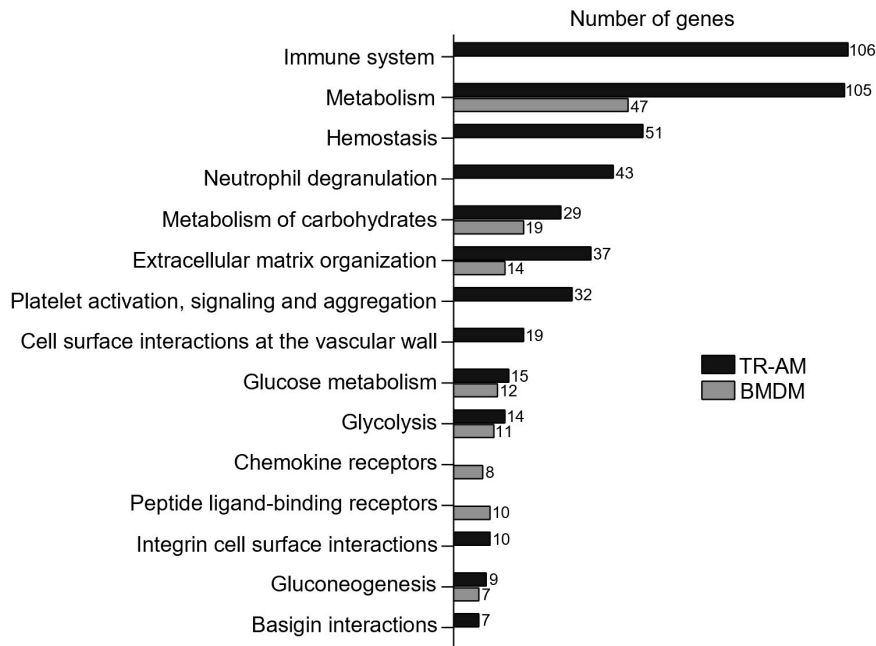
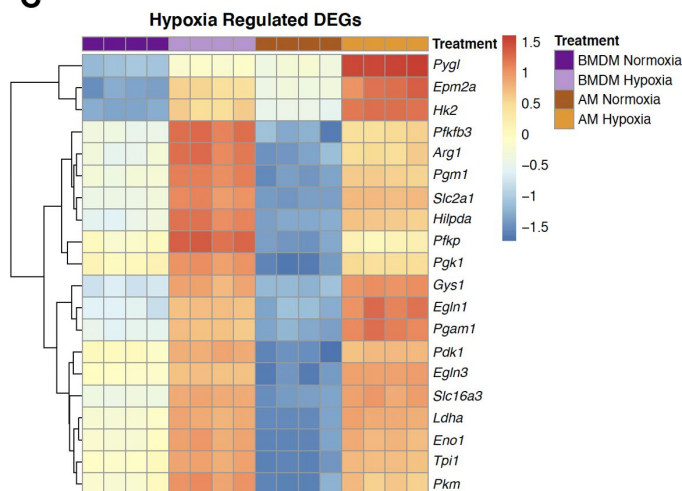
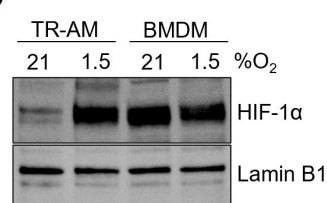
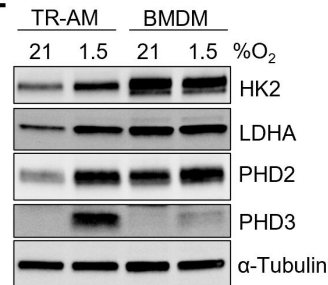


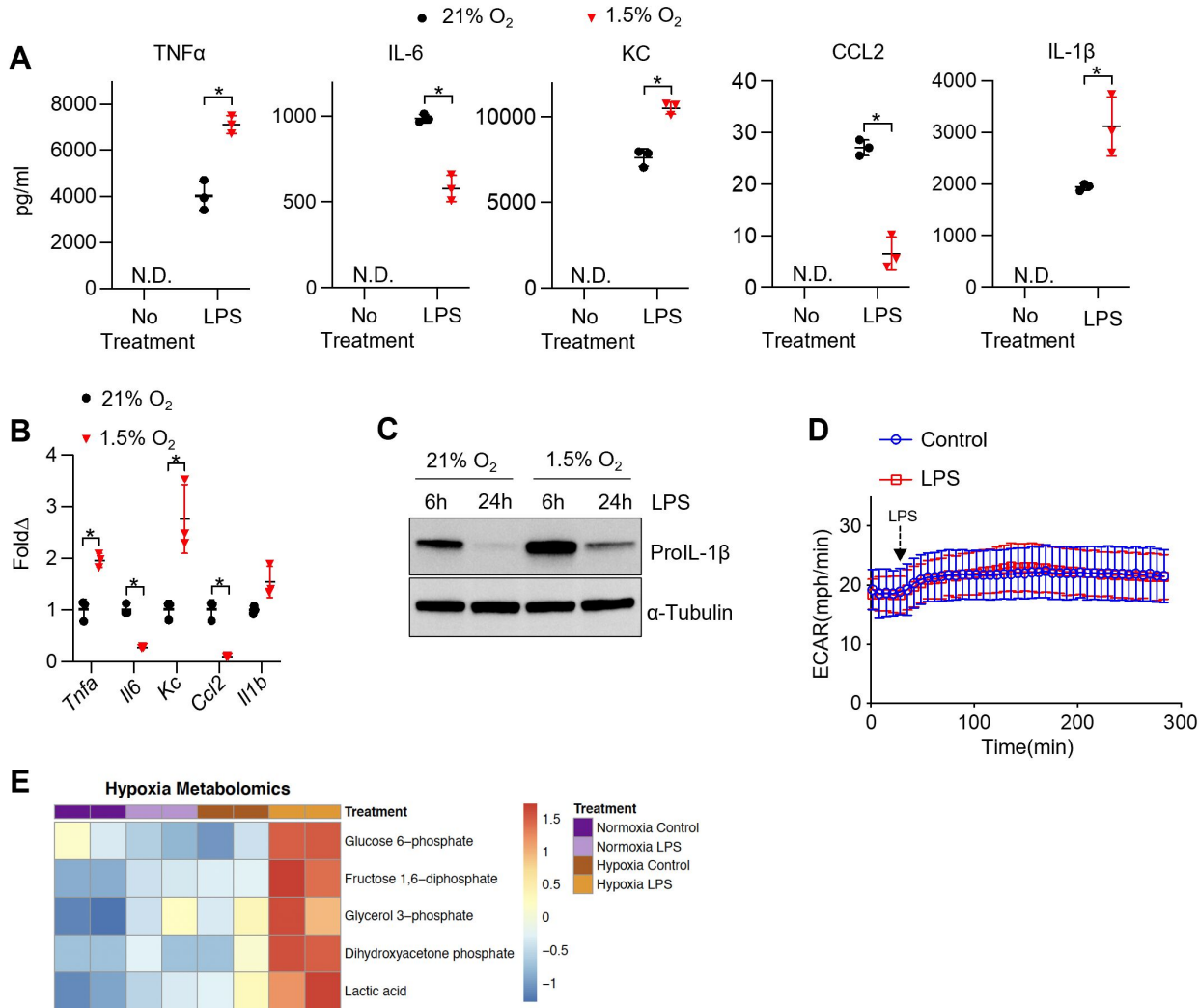
A**B****C****D****E****F**

A**B****C****D****E****F**

A**B**

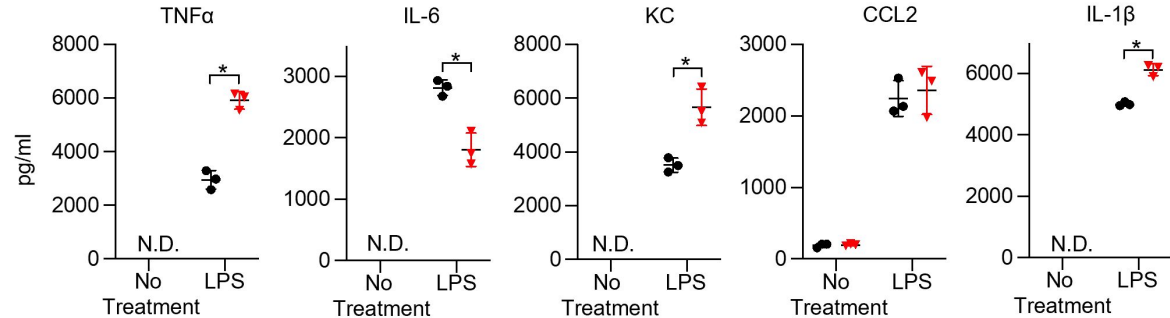
Normoxia vs Hypoxia (1.5% O₂)
Reactome Pathways (P<0.001 and FDR<0.05)

**C****D****E**



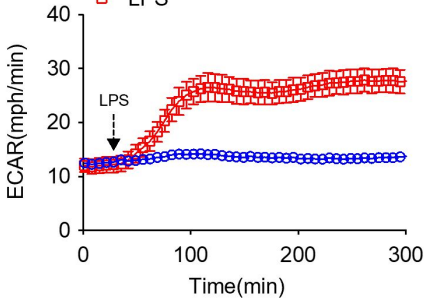
● 21% O₂

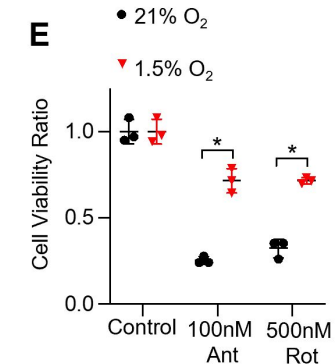
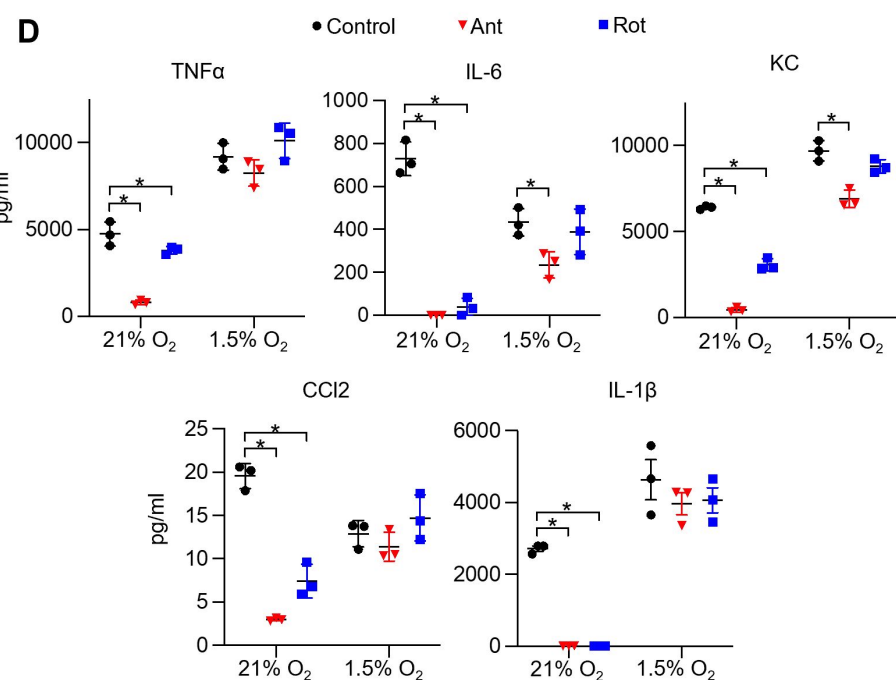
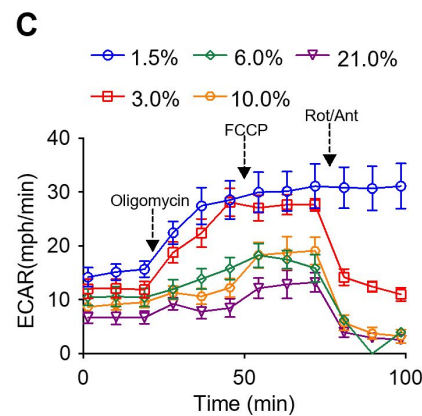
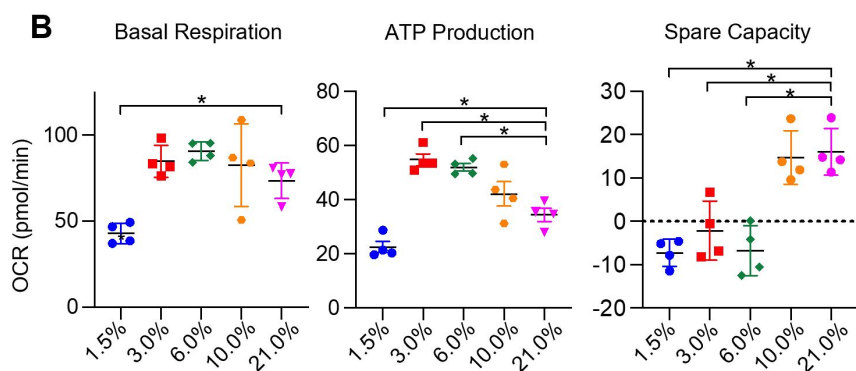
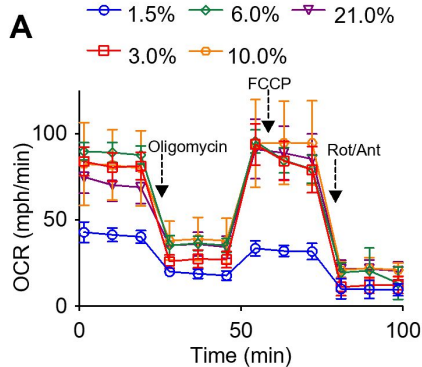
▼ 1.5% O₂

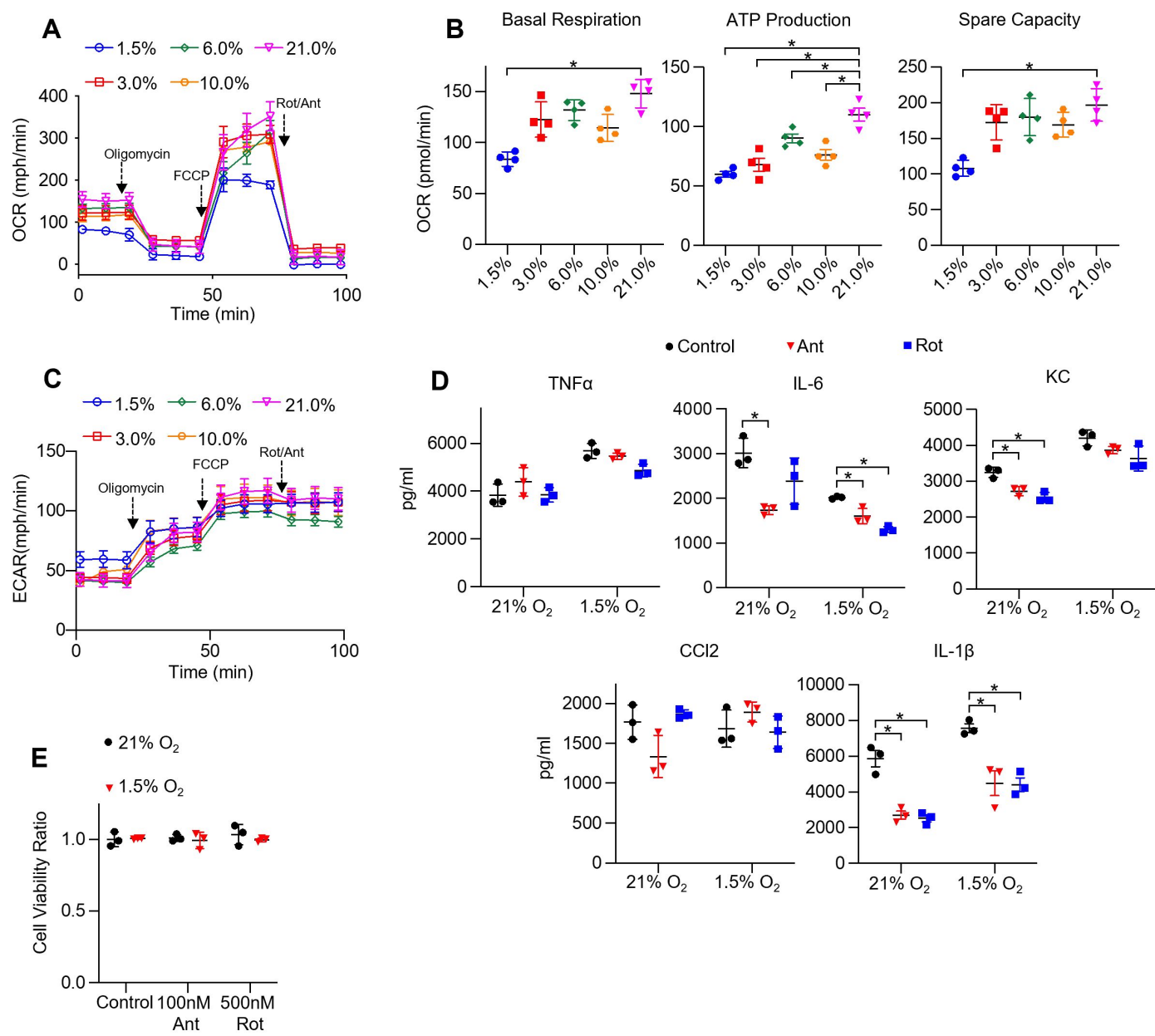


Control

LPS

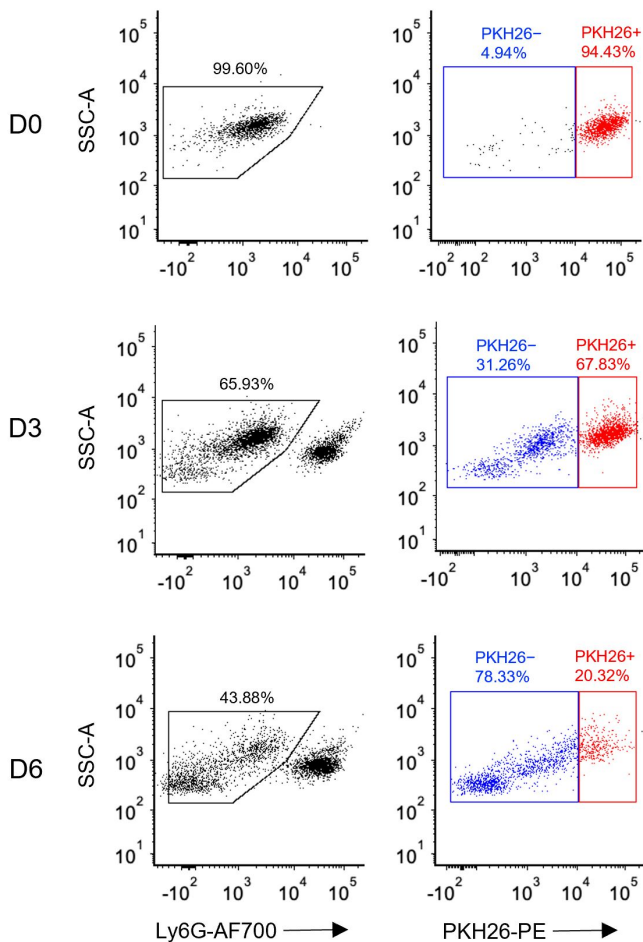




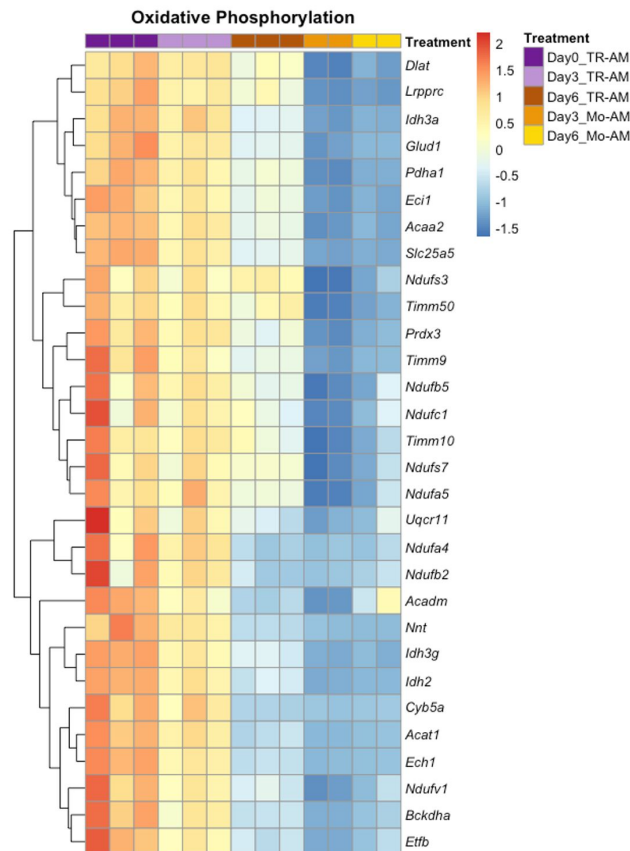


■ TR-AMs (PKH26+)
■ Mo-AMs (PKH26-)

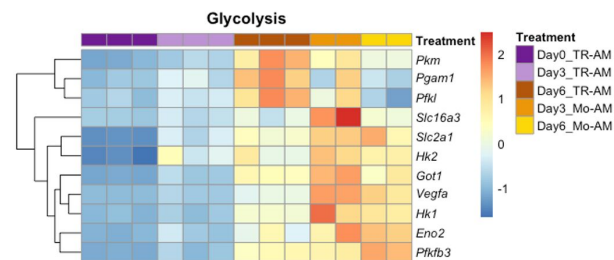
A

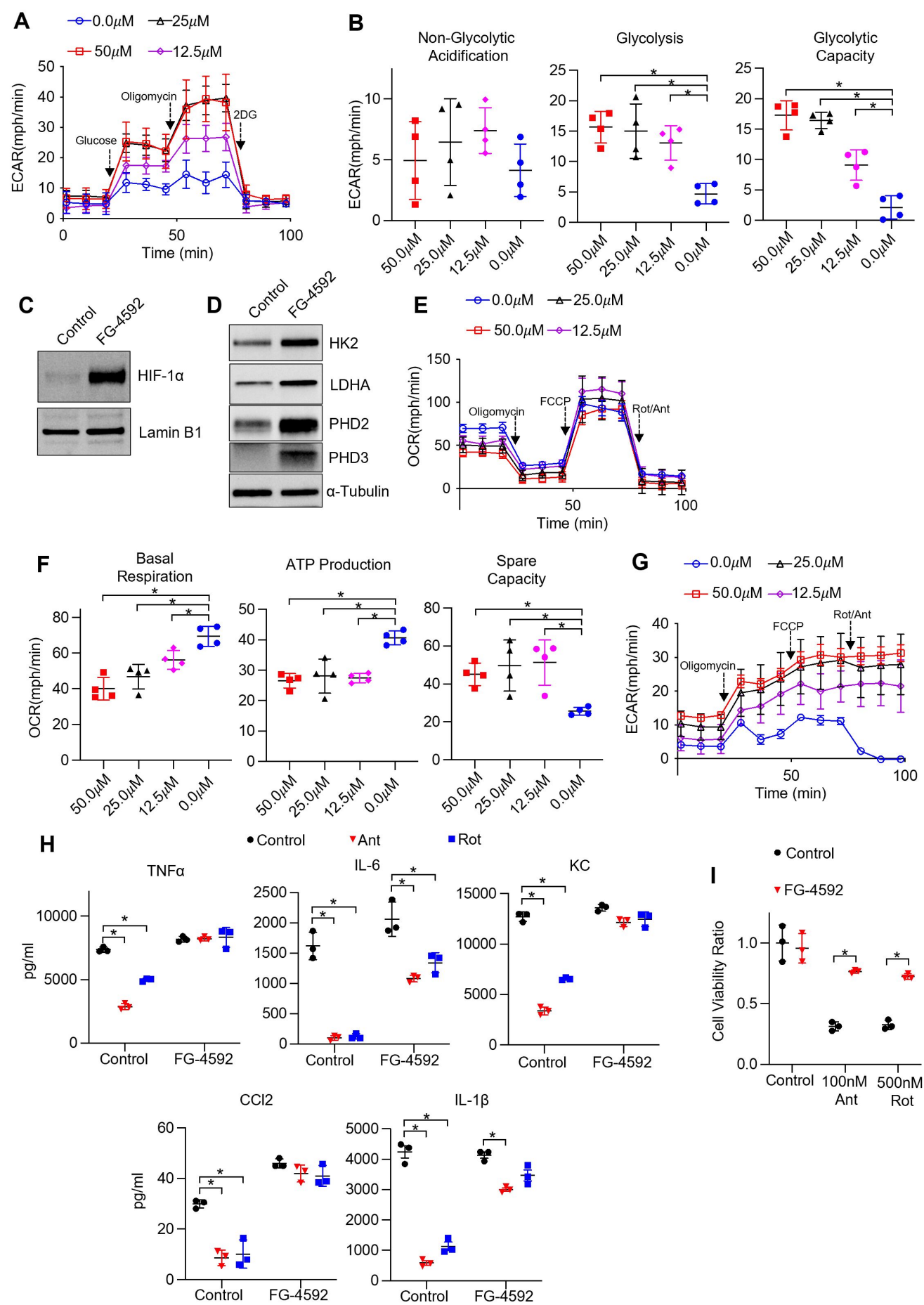


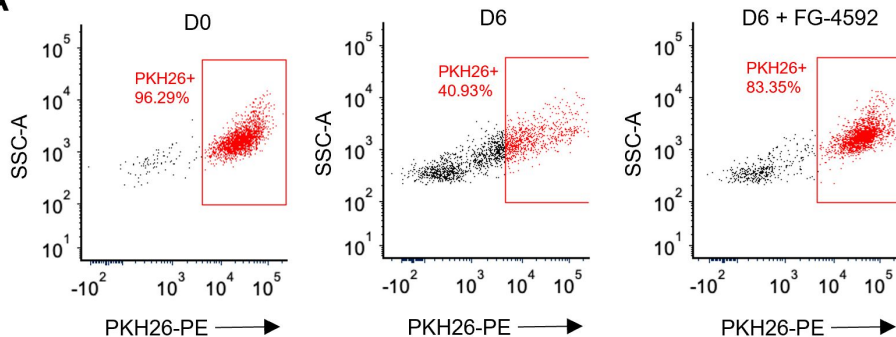
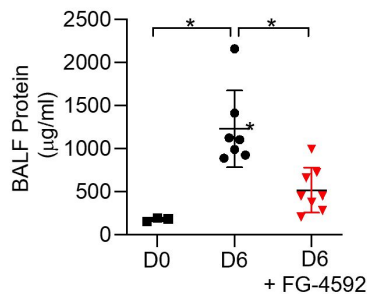
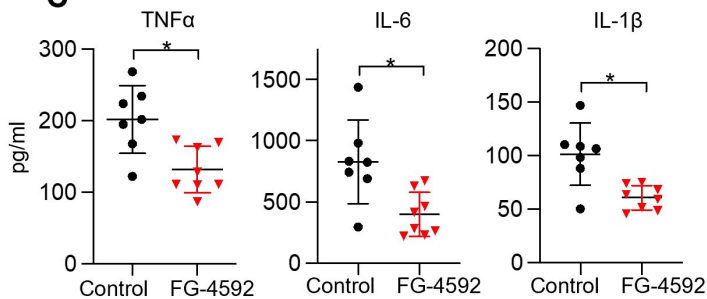
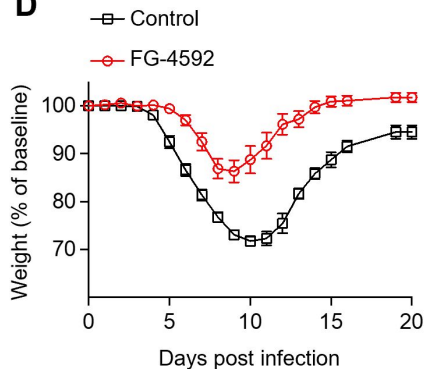
B



C





A**B****C****D****E**